Middle-late Pleistocene deep water circulation in the southwest subtropical Pacific

T. Russon,[1] M. Elliot,[1] C. Kissel,[2] G. Cabioch,[3,4] P. De Deckker,[5] and T. Corrège[6]

Received 19 February 2009; revised 9 June 2009; accepted 17 July 2009; published 27 October 2009.

[1] The modern $\delta^{13}C_{DIC}$ distribution in southwest subtropical Pacific deep waters is consistent with a regional mixing regime between water masses of open Pacific Ocean and Tasman Sea origin. This mixing regime is reconstructed across the middle-late Pleistocene using a record of benthic foraminiferal $\delta^{13}C$ in a sediment core from the New Caledonia Trough. The relative influence on the mixing regime from open Pacific Ocean deep waters is seen to be significantly reduced during glacial in comparison to interglacial stages over the past 1.1 Ma. The spatial $\delta^{13}C$ gradient in the Southern Ocean between deep waters entering the Tasman Sea and the open Pacific Ocean is shown to be consequently greater during glacial than interglacial stages but was generally reduced across the period of the Middle Pleistocene Transition. The existence of strong spatial chemical gradients in the glacial Southern Ocean limits its capacity to act as an enhanced sink for atmospheric carbon.

Citation: Russon, T., M. Elliot, C. Kissel, G. Cabioch, P. De Deckker, and T. Corrège (2009), Middle-late Pleistocene deep water circulation in the southwest subtropical Pacific, *Paleoceanography*, *24*, PA4205, doi:10.1029/2009PA001755.

1. Introduction

[2] The majority of the inorganic carbon in the ocean/atmosphere system resides in the deep waters of the global ocean. The modern residency time for these waters is of the order of 1000–2000 years meaning that changes in deep water circulation have the potential to play a key role in driving and propagating climatic change on centennial, millenial [*Elliot et al.*, 2002; *Pahnke and Zahn*, 2005] and glacial-interglacial timescales [*Archer et al.*, 2000; *Charles and Fairbanks*, 1992; *Piotrowski et al.*, 2005]. On longer timescales, changes in the mean state of regional and global deep water circulation regimes both contribute to and are diagnostic of different states in the evolution of Plio-Pleistocene climate [*Raymo et al.*, 1997].

[3] Past deep water circulation patterns may be reconstructed using proxy measurements of chemical properties characteristic of certain water masses. One such proxy is the isotopic composition of carbon in benthic foraminiferal calcite ($\delta^{13}C_{benthic}$) which reflects the isotopic composition of dissolved inorganic carbon ($\delta^{13}C_{DIC}$) in the overlying water mass. The $\delta^{13}C_{DIC}$ of deep water depends on the chemistry of the source region for that water mass and $\delta^{13}C_{benthic}$ measurements can therefore be used to reconstruct past water mass distributions. However, deep water $\delta^{13}C_{DIC}$ is also affected by whole ocean chemistry changes on a range of timescales. On the glacial-interglacial timescale, fluctuations in the terrestrial biomass lead to mean ocean $\delta^{13}C_{DIC}$ changes [*Crowley*, 1995; *Shackleton*, 1977]. During the Middle Pleistocene Transition (MPT), 500–1200 ka [*Head and Gibbard*, 2005], the dominant glacial-interglacial periodicity changed from 41 kyr to 100 kyr [*Berger and Jansen*, 1994; *Maasch and Saltzman*, 1990; *Mudelsee and Stattegger*, 1997] and global mean ocean $\delta^{13}C_{DIC}$ shows a ~500 kyr perturbation toward more negative values [*Raymo et al.*, 1997].

[4] The deep open Pacific Ocean is the largest reservoir of dissolved inorganic carbon on the planet and Pleistocene records of deep equatorial Pacific $\delta^{13}C_{benthic}$ show the lowest amplitude of glacial-interglacial variability of any major ocean basin [*Raymo et al.*, 1997]. This variability is close to estimates of the mean ocean glacial-interglacial $\delta^{13}C_{DIC}$ change [*Crowley*, 1995]. In the modern open Pacific circulation regime, all deep water originates from the Southern Ocean as there is no ventilation of deep waters anywhere in the open Pacific itself. However, reconstructions of Pacific-wide $\delta^{13}C_{DIC}$ distributions at the Last Glacial Maximum (LGM) suggest that a very different circulation regime may have been active, possibly involving the ventilation of deep waters in the North Pacific [*Curry et al.*, 1988; *Keigwin*, 1998] and/or radical changes in Southern Ocean deep water formation and circulation [*Hodell et al.*, 2003; *Michel et al.*, 1995; *Ninnemann and Charles*, 2002]. In the modern Southern Ocean, the Antarctic Circumpolar Current effectively homogenizes deep waters down to the seafloor, but at the LGM reconstructions suggest that enhanced vertical $\delta^{13}C_{DIC}$ gradients existed in the region [*Hodell et al.*, 2003]. Such an increase in the stratification of the deep Southern Ocean is potentially an important mechanism in lowering glacial stage pCO_2

[1]School of Geosciences, University of Edinburgh, Edinburgh, UK.
[2]Laboratoire des Sciences du Climat et de l'Environnement, IPSL, Laboratoire Mixte CEA-CNRS-UVSQ, Parc du CNRS, Gif-sur-Yvette, France.
[3]Institut de Recherche pour le Développement, Unité de Recherche Paléotropique, Nouméa, New Caledonia.
[4]Now at LOCEAN, UMR 7159, IRD, UPMC, MNHN, CNRS, Bondy, France.
[5]Research School of Earth Sciences, Australian National University, Canberra, ACT, Australia.
[6]Environnements et Paléoenvironnements Océaniques, UMR 5805, Université de Bordeaux, CNRS, Bordeaux, France.

0883-8305/09/2009PA001755$12.00

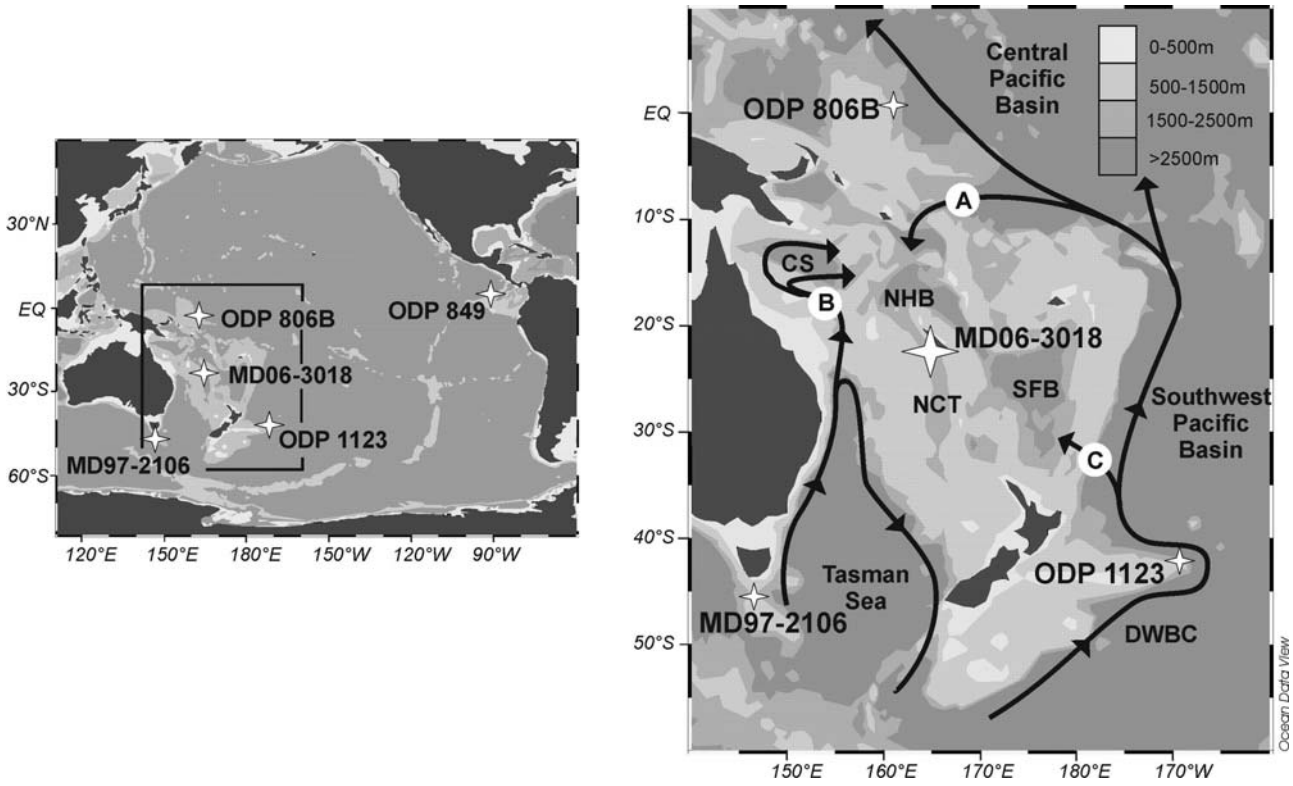

Figure 1. (left) Map of Pacific Ocean region with core locations mentioned in text. (right) Bathymetric map of the SWSP region with the location of cores MD06−3018, ODP 1123, and ODP 806B. Bathymetry from WOCE Ocean Atlas [*Talley*, 2007; *WOCE*, 2002] viewed in Ocean Data View software (R. Schlitzer, Ocean Data View, 2007, available at http://odv.awi.de). Arrows indicate dominant directions of bottom water flow, adapted from *Sokolov and Rintoul* [2000]. Lettered arrows refer to flow paths described in text. NCT, New Caledonia Trough; NHB, New Hebrides Basin; SFB, South Fiji Basin; CS, Coral Sea; DWBC, Deep Western Boundary Current.

[*Hodell et al.*, 2003; *Sigman and Boyle*, 2000; *Toggweiler*, 1999].

[5] The southwest subtropical Pacific (SWSP), taken here as consisting of the Coral Sea, the Solomon Sea, the New Hebrides Basin, the New Caledonia Trough, and the South Fiji Basin is bounded to the north and east by the basins of the open Pacific Ocean and to the south by the Tasman Sea which opens in turn into the Southern Ocean. In the modern deep water circulation regime, water masses from the Central Pacific Basin, Tasman Sea, and Southwest Pacific Basin all enter the SWSP region (Figure 1) leading to a deep water mixing regime sensitive to the chemistry of both open Pacific Ocean and Tasman Sea deep waters [*Tsimplis et al.*, 1998; *Warren et al.*, 1994; *Wyrtki*, 1961].

[6] The present study evaluates how the SWSP deep water mixing regime has evolved across the middle-late Pleistocene, specifically whether it is variable between glacial and interglacial stages and whether it persists across the climatic shift of the MPT. It is first demonstrated that the modern $\delta^{13}C_{DIC}$ chemistry of SWSP deep waters is consistent with the modern mixing regime. A $\delta^{13}C_{benthic}$ record from a recently obtained sediment core located at 2470 m depth in the New Caledonia Trough, in comparison with other regional records, is then used to reconstruct the relative influences of open Pacific Ocean and Tasman Sea deep waters on the mixing regime. Reconstruction of the mixing regime allows constraints to be placed on past deep water chemical gradients between the different regions of the Southern Ocean from which the Tasman Sea and open Pacific Ocean deep waters originate.

2. Materials and Methods

2.1. Core Location

[7] Deep sea sediment core MD06−3018 was recovered from 2470 m water depth on the eastern side of the New Caledonia Trough (NCT), ~60 km offshore of the island of New Caledonia (Figure 1 and Table 1) during cruise AUSFAIR/ZoNéCo12 on board the R.V. *Marion Dufresne* [*Foucher et al.*, 2006]. The core is 24.5 m long and composed entirely of foraminifera-rich calcareous ooze. The NCT is one of a series of broadly NW-SE trending basins in the SWSP region [*Lafoy et al.*, 2005; *Pelletier*, 2006], lying between the Lord Howe Rise to the west and the Norfolk Ridge to the east. It is open to a sill depth of ~3000 m into the New Hebrides Basin to the north, attains its deepest depths near to New Caledonia itself (~3600 m) and shallows to the south as it approaches New Zealand [*Lafoy et al.*, 2005; *Wyrtki*, 1961].

Table 1. Sediment Core Records

Core	Latitude	Longitude	Water Depth	Taxa Used for $\delta^{13}C_{benthic}$ Measurements	References
MD06-3018	23°00′S	166°09′E	2470 m	*Cibicides wuellerstorfi*	Present study
ODP 1123	41°47′S	171°20′W	3290 m	*Uvigerina* spp	*Hall et al.* [2001] *Harris* [2002]
ODP 806B	0°19′N	159°22′E	2520 m	*Cibicides wuellerstorfi*	*Bickert et al.* [1993]
ODP 849	0°11′N	110°31′W	3840 m	*Cibicides wuellerstorfi* and *Uvigerina* spp	*Mix et al.* [1995]
MD97-2106	45°09′S	146°17′E	3310 m	*Cibicides* spp	*Moy et al.* [2006]

2.2. Modern Deep Water Circulation and Mixing in the SWSP

[8] At surface and intermediate water depths, the SWSP forms an integral part of the South Pacific gyre system. Surface waters in the NCT are influenced both by the South Equatorial Current and the East Australian Current which transports warm waters from the Western Pacific Warm Pool region southward to the Tasman Front [*Bostock et al.*, 2006; *Ridgway and Dunn*, 2003]. Predominantly westward flowing Antarctic Intermediate Water (AAIW) enters the region both to the north and south of New Caledonia [*Gourdeau et al.*, 2008]. Below the depths of AAIW, however, the bathymetry of the region means that deep water exchange with the larger adjacent basins of the Tasman Sea and the open Pacific Ocean is restricted.

[9] The Southern Ocean is the source of all modern deep waters in both the open Pacific Ocean and the Tasman Sea. These deep waters enter the open Pacific Ocean principally via the Deep Western Boundary Current (DWBC) in the Southwest Pacific Basin [*Whitworth et al.*, 1999] (Figure 1). The deep water entering both the Pacific DWBC and the southern Tasman Sea consists of Lower Circumpolar Deep water (LCDW) overlain by Upper Circumpolar Deep Water (UCDW). LCDW is characterized by salinities of 34.71–34.73 psu and dissolved oxygen concentrations of ~200 μmol/kg. It may be subdivided into upper LCDW (uLCDW), characterized by a salinity maximum related to the presence of relict North Atlantic Deep Water [*Gordon*, 1975; *Warren*, 1981; *Wijffels et al.*, 2001] and lower LCDW (lLCDW) which consists of Southern Ocean origin deep and bottom waters [*Rintoul*, 1998]. The northward flow of LCDW is kept balanced on a Pacific-wide scale by the net southward return flow at depths of 1500–3000 m of chemically aged North Pacific Deep Water (NPDW) which is characterized by salinities of 34.65–34.66 psu and dissolved oxygen concentrations of <150 μmol/kg [*Reid*, 1997]. UCDW has similar properties to NPDW as it consists of recirculated NPDW and Indian Ocean deep waters that have been entrained into the DWBC [*Gordon*, 1975; *McCave et al.*, 2008].

[10] Deep waters below ~2000 m in the NCT are net southward flowing and originate in the New Hebrides Basin [*Reid*, 1997; *Tsimplis et al.*, 1998; *Wyrtki*, 1961] (Figure 1). They are characterized at 2500 m depth by salinities of ~34.68 psu and dissolved oxygen concentrations of ~160 μmol/kg (Figure 2c, station P06–215). The dominant modern deep water inflow to the New Hebrides Basin is from the Central Pacific Basin (Figure 1, arrow A) to which it is open down to 3000 m [*Sokolov and Rintoul*, 2000; *Wijffels et al.*, 2001]. Central Pacific Basin deep waters in the depth range 2000–3000 m are characterized by salinities of 34.65–34.66 psu and dissolved oxygen concentrations of 130–140 μmol/kg, consistent with a UCDW/NPDW origin (Figure 2c). The NCT deep water properties are too chemically young and too saline to be explained purely from an open Pacific Ocean source. Instead, NCT deep waters represent the product of a mixing regime between deep waters from the open Pacific Ocean and the Tasman Sea (Figure 1, arrow B), as first described by *Wyrtki* [1961]. The Tasman Sea inflow occurs over a sill depth at 2850 m into the Coral Sea [*Wijffels et al.*, 2001] and is poorly constrained volumetrically, having been estimated as both 0.05 Sv [*Wyrtki*, 1961] and 3.0 Sv [*Sokolov and Rintoul*, 2000]. The contact between UCDW/NPDW and uLCDW is substantially shallower in the Tasman Sea than in the DWBC region (Figure 2c). This means that the deep waters entering the SWSP from the Tasman Sea at ~2500 m depth lie close to the core of the Tasman Sea uLCDW with salinities of ~34.72 psu dissolved oxygen concentrations of ~180 μmol/kg (Figure 2c, station P06–234). The influence of the chemically younger and more saline Tasman Sea deep water declines eastward across the SWSP region but remains detectable in the New Hebrides Basin and the NCT [*Wyrtki*, 1961].

[11] Subsequent conservative tracer work as part of the SCORPIO and WOCE projects [*Sokolov and Rintoul*, 2000; *Tsimplis et al.*, 1998; *Warren*, 1973; *Wijffels et al.*, 2001] has not changed this basic picture although the South Fiji Basin has been shown to receive a small (~0.2 Sv) inflow (Figure 1, arrow C) of DWBC water directly from the Southwest Pacific Basin over a sill depth of less than 2500 m [*Warren et al.*, 1994].

2.3. Modern Deep Water Mass $\delta^{13}C_{DIC}$ in the SWSP

[12] Deep water masses may potentially be characterized by their $\delta^{13}C_{DIC}$ signatures due to variations in the isotopic composition of the source regions for the deep waters and the general inverse relationship between $\delta^{13}C_{DIC}$ and nutrient concentrations [*Charles and Fairbanks*, 1992; *Duplessy et al.*, 1988; *Kroopnick*, 1985]. Comparison of modern $\delta^{13}C_{DIC}$, dissolved oxygen and salinity measurements from WOCE stations in the SWSP region demonstrates that the same deep water masses definable on the basis of the conservative tracers are also visible in the corresponding $\delta^{13}C_{DIC}$ profiles (Figure 2c).

[13] Modern $\delta^{13}C_{DIC}$ values at 2500 m depth in the NCT (station P06–215) are 0.25‰, with an analytical reproducibility of ±0.03‰. These are similar to the values of 0.23‰ seen at the same depth and latitude in the Southwest Pacific Basin (station P06–168). The direct deep water inflow from the Southwest Pacific Basin into the SWSP (Figure 1, arrow C) cannot account for this similarity as it occurs over a sill depth shallower than 2500 m [*Warren et*

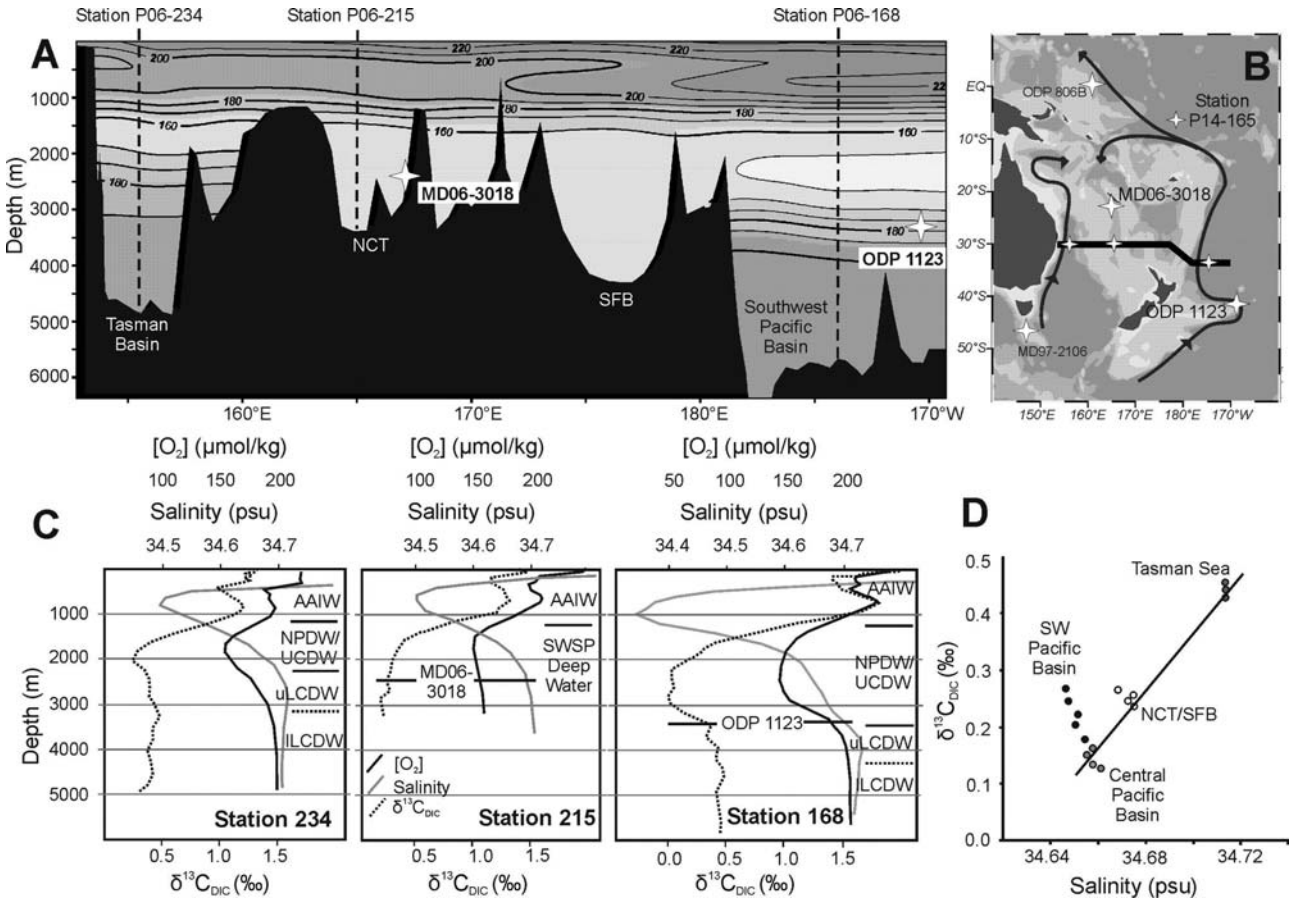

Figure 2. (a) Dissolved [O_2] section across the SWSP region along WOCE P06W section line. The longitudinal positions and water depths of MD06−3018 and ODP 1123 are shown although both core sites are off the section line. (b) Location of WOCE P06W section line (bold line) and WOCE stations (white stars) referred to in the text in relation to the dominant deep water pathways. (c) Dissolved [O_2] (solid black lines), salinity (solid gray lines), and $\delta^{13}C_{DIC}$ (dotted lines) profiles from the Tasman Sea (station P06−234), New Caledonia Trough (station P06−215), and the Southwest Pacific Basin (station P06−168). The main intermediate and deep water masses as seen in [O_2] and salinity are highlighted. AAIW, Antarctic Intermediate Water; NPDW, North Pacific Deep Water; UCDW, Upper Circumpolar Deep Water; uLCDW, upper Lower Circumpolar Deep Water; lLCDW, lower Lower Circumpolar Deep Water. (d) Scatterplot and mixing line plot of salinity against $\delta^{13}C_{DIC}$ at 2500 ± 100 m depth for WOCE P06W, P14S, and P15S stations with available $\delta^{13}C_{DIC}$ measurements. The line represents a two end-member mixing regime of central Pacific Basin and Tasman Seawater. CTD and bottle data from the WOCE Pacific Ocean Atlas [*Johnson et al.*, 2001; *Key et al.*, 2004; *McTaggart et al.*, 1994; *McTaggart and Johnson*, 1997; *Talley*, 2007; *Tsimplis et al.*, 1998; *Wijffels et al.*, 2001; *WOCE*, 2002] viewed in Ocean Data View software (R. Schlitzer, Ocean Data View, 2007, available at http://odv.awi.de).

al., 1994]. Instead, the dominant inflow from the open Pacific occurs through the Central Pacific Basin (Figure 1, arrow A). Deep water at 2500 m depth in the Southwest Pacific and Central Pacific Basins becomes progressively lighter in $\delta^{13}C_{DIC}$ toward the equator due principally to the increasing relative influence of NPDW over UCDW (Figure 2d). The values of 0.12‰ seen in the southern Central Pacific Basin (station P14−165) are significantly lighter than those seen in the NCT. Thus, as with the conservative tracers, the NCT $\delta^{13}C_{DIC}$ values cannot be explained from a purely open Pacific deep water source.

[14] The positive NCT deep water $\delta^{13}C_{DIC}$ values do not arise from vertical mixing with AAIW ($\delta^{13}C_{DIC}$ ~1‰) as there is no evidence for downward penetration of the AAIW salinity minima to depths of 2500 m at station P06−215. However, modern $\delta^{13}C_{DIC}$ values in northern Tasman Sea deep waters at 2500 m are 0.42‰ (station P06−234) sufficiently positive to provide a viable second end-member to the deep water mixing regime.

[15] The regional mixing relationship derived from the $\delta^{13}C_{DIC}$ values along the isopycnal corresponding to water at 2500 m depth in the NCT is consistent with that seen for the corresponding salinities (Figure 2d). This suggests that proxy records of past deep water $\delta^{13}C_{DIC}$ may be used to reconstruct the regional mixing regime. Using this simple model, modern NCT deep waters are seen to be a roughly

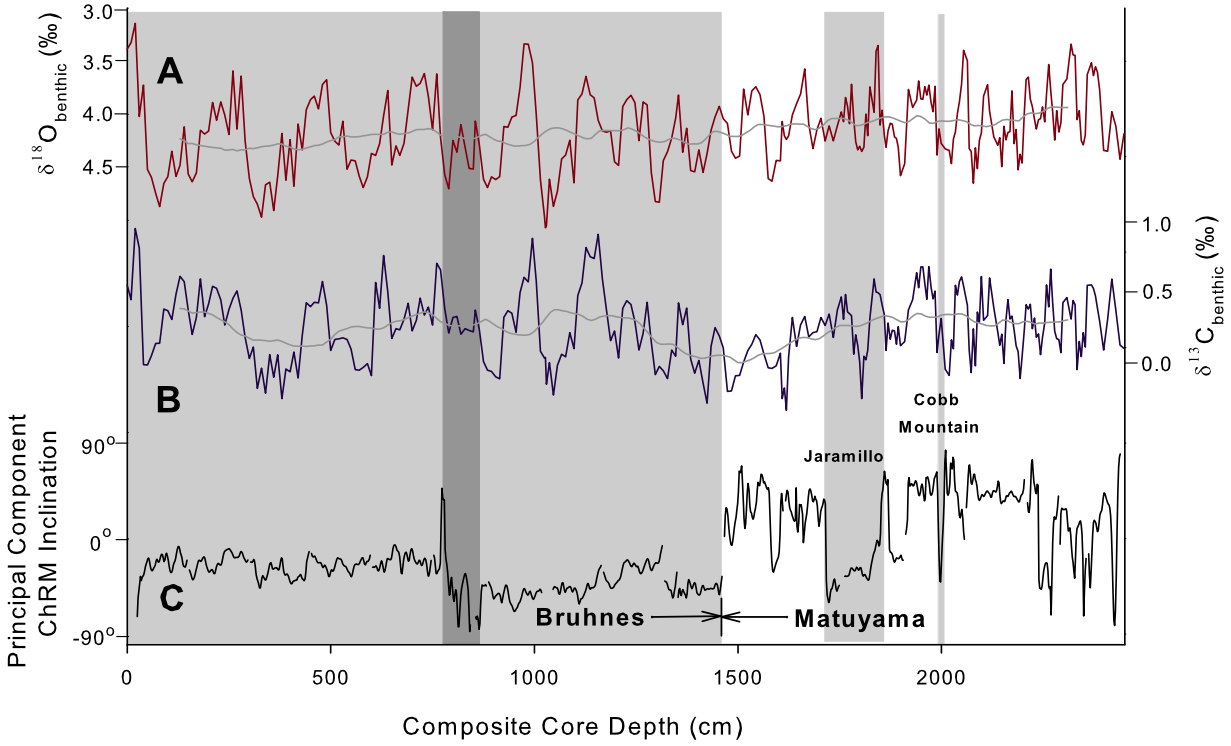

Figure 3. Plot of (a) $\delta^{18}O_{benthic}$ (gray line is 250 cm linear smoothed mean value), (b) $\delta^{13}C_{benthic}$ (gray line is 250 cm linear smoothed mean value), and (c) principal component of ChRM Inclination from MD06–3018 against depth. The positions of identified magnetic reversals and events are highlighted with light gray boxes representing periods of normal polarity. The dark gray box at 755–840 cm depth highlights a period of disturbed sedimentation.

2:1 admixture of Central Pacific Basin UCDW/NPDW and Tasman Sea uLCDW.

2.4. Stable Isotope Measurements

[16] Core MD06–3018 was sampled at 10 cm intervals for core depths 0–1800 cm and 5 cm intervals for 1800–2490 cm. Samples were wet sieved and the >150 μm fraction collected and dried for subsequent analysis. Monospecific samples of the epibenthic foraminifera *Cibicides wuellerstorfi* (3–6 individuals from the >315 μm size fraction) were picked under the microscope and subsequently placed for 5 s in an ultrasonic bath with methanol. Samples were analyzed with a Thermo Electron Delta+ Mass Spectrometer with Kiel Preparation Device in the School of Geosciences, University of Edinburgh for $\delta^{18}O$ and $\delta^{13}C$. Long-term accuracy (against an internal standard calibrated to NBS19) of the device (May 2006 to October 2008) was 1σ = 0.09‰ for $\delta^{18}O$ and 0.08‰ for $\delta^{13}C$. Replicate analyses ($3 < n < 6$) were performed at six intervals downcore, the one standard deviation measurement reproducibility (σ_m) was always better than 0.13‰ for $\delta^{18}O$ and 0.16‰ for $\delta^{13}C$. *C. wuellerstorfi* $\delta^{18}O$ values are corrected by the standard +0.64‰ to account for disequilibrium with the surrounding seawater [*Shackleton and Opdyke*, 1973]. All isotopic values are quoted relative to VPDB.

2.5. Magnetic Measurements

[17] Measurements of Natural Remnant Magnetization (NRM) were made on u-channel samples taken in the central part of the half core. The measurements were performed in the shielded room at the Laboratoire des Sciences du Climat et de l'Environnement (LSCE) using the 2G-pass-through cryogenic magnetometer equipped with high-resolution coils. Measurements were taken every 2 cm with a resolution of 4 cm inducing a slight smoothing of the signal. The data from the extreme 3 cm at the ends of each core section are not presented due to edge effects. The NRM was stepwise demagnetized at 5, 10, 15, 20, 25, 30, 35, 40, 45, 50, 60, and 80 mT. The Characteristic Remnant magnetization (ChRM) was then determined using principal component analysis [*Mazaud*, 2005]. Nine steps out of thirteen have been taken into account to define the ChRM with mean angular deviations ranging between 5° and 10° (a few horizons reach 20°).

3. Results

3.1. Stable Isotopes

[18] The $\delta^{18}O_{benthic}$ record (Figure 3a) shows a succession of well-defined cycles on the 50–250 cm scale with average amplitude of 1.2‰ in the section 0–1100 cm and amplitudes in the range 0.5–0.7‰ below 1100 cm. The running mean value (250 cm linear smoothing using a boxcar method) of $\delta^{18}O_{benthic}$ is in the range 4.15 ± 0.15‰ across the length of the record.

[19] The $\delta^{13}C_{benthic}$ record (Figure 3b) shows variability on the 50–250 cm scale with average amplitude of 0.8‰ in

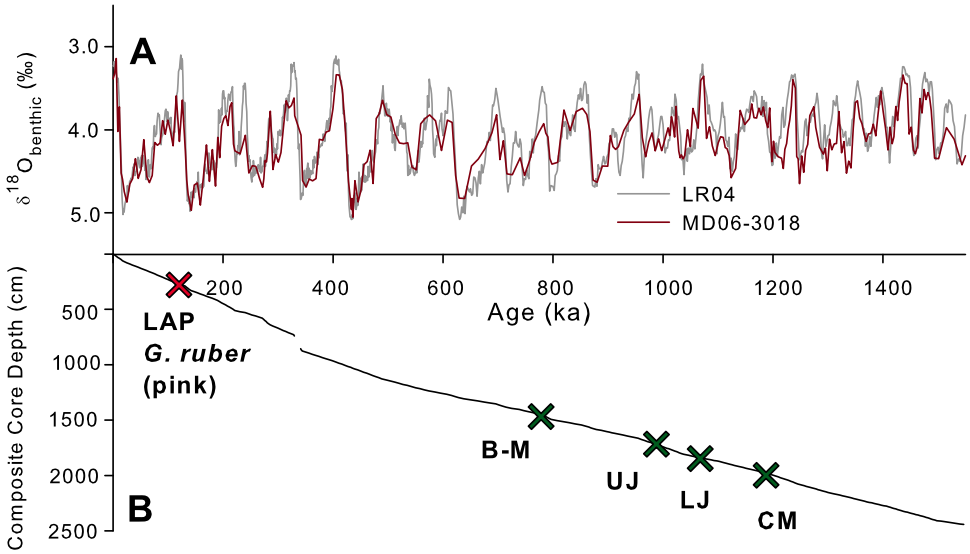

Figure 4. (a) Comparison of $\delta^{18}O_{benthic}$ from LR04 and MD06–3018 used in development of tuned age model. (b) LR04 age model. Crosses represent the four identified magnetic tie points (B-M, Bruhnes-Matuyama; UJ, Upper Jaramillo; LJ, Lower Jaramillo; CM, Centre Cobb Mountain Event) and the last appearance (LAP) of *G. ruber* (pink). Gap in the age model arises from the interval of disturbed sedimentation at 740–855 cm.

the section 0–1250 cm and average amplitude of 0.5‰ below 1250 cm. The running mean value (250 cm linear smoothing using a boxcar method) of $\delta^{13}C_{benthic}$ is in the range 0.25 ± 0.15‰ across the sections 0–1250 cm and 1800–2450 cm but undergoes a negative perturbation toward a minimum value of 0.0‰ during the intervening section.

3.2. Magnetic Measurements

[20] The ChRM Inclination record (Figure 3c) shows a series of reversals between positive (reversed polarity) and negative (normal polarity) inclination. The section between the core top and 1500 cm has consistently negative inclination and corresponds to the Bruhnes Chron followed by a period of overall positive inclination corresponding to the Matuyama Chron. Within the Matuyama Chron, the beginning and end of the Jaramillo reversal and the midpoint of the shorter Cobb Mountain reversal are identified [*Laj and Channell*, 2007].

3.3. Age Model

[21] An age model for MD06–3018 was developed based on both the magnetic stratigraphy (Figure 3c) and orbital tuning of the $\delta^{18}O_{benthic}$ record with the LR04 stack [*Lisiecki and Raymo*, 2005] (Figure 4) using the Analyseries software package [*Paillard et al.*, 1996]. The magnetic boundary dates used are those of the ODP677 calibration [*Cande and Kent*, 1995; *Shackleton et al.*, 1990]. The orbital age model yields average sedimentation rates of 25 mm/ka in the section 0–740 cm and 15 mm/ka in the section 855–2450 cm. The magnetic tie points are highly consistent with the orbital age model (Figure 4). An additional tie point at 280 cm based on the disappearance of *Globigerinoides ruber* (pink) from the Pacific at 120 ka [*Thompson et al.*, 1979] is also in close agreement with the orbital model.

[22] The interval 740–855 cm shows signs of enhanced vertical mixing in the physical properties of the core, the presence of shallow-water benthic foraminifera taxa, perturbations to the ChRM Inclination record and a lack of reproducibility in the $\delta^{18}O_{benthic}$ measurements (Figure 3). The data from this interval is likely to be contaminated with downslope signals and is excluded from the development of the core age model (Figure 4). The section below 2230 cm also shows high variability in the ChRM Inclination record not associable with any known magnetic event but without additional accompanying evidence of sediment disturbance, leading to a reduction in age model confidence below 2230 cm (1.36 Ma).

[23] The sampling resolution based on the orbital age model is always better than 6 kyr and each 1 cm sample thickness represents time averaging of 450–600 years. When plotted against the core age model the $\delta^{18}O_{benthic}$ data (Figure 5a) allows the identification of marine isotope stages (MIS) as far back as MIS 51, the core bottom being at 1.54 Ma. The shift in dominant glacial-interglacial frequency during the MPT is evident in both the $\delta^{18}O_{benthic}$ and $\delta^{13}C_{benthic}$ records when plotted against the age model (Figure 5) and occurs over the same interval as the negative perturbation in mean value seen in the $\delta^{13}C_{benthic}$ record.

4. Discussion

4.1. Does $\delta^{13}C_{benthic}$ at Site MD06–3018 Record $\delta^{13}C_{DIC}$?

[24] The $\delta^{13}C_{benthic}$ of *C. wuellerstorfi* is widely held to be a reliable direct recorder of bottom water $\delta^{13}C_{DIC}$ [*Curry and Lohmann*, 1982; *Duplessy et al.*, 1984; *McCorkle and*

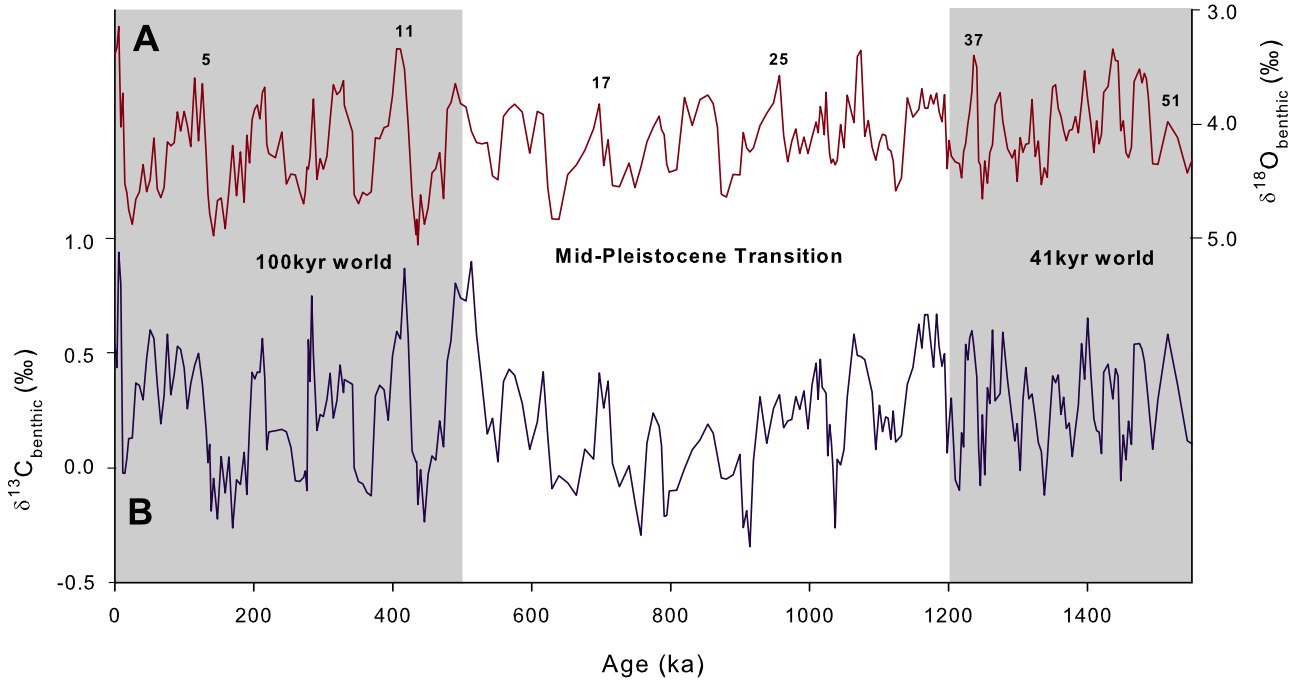

Figure 5. MD06–3018 (a) $\delta^{18}O_{benthic}$ with numbers referring to selected interglacial marine isotope stages and (b) $\delta^{13}C_{benthic}$ plotted against the core age model. MPT interval is marked with light shading as 500–1200 ka, using the generalized boundary dates of *Head and Gibbard* [2005].

Keigwin, 1994; *Shackleton and Opdyke*, 1973]. The absence of a well-preserved core top in MD06–3018 means that direct verification of this relationship at the core site is not possible. An average of four $\delta^{13}C_{benthic}$ measurements with age model values in the range 0–5 ka yields a late Holocene value of $0.56 \pm \sigma_{SEM} = 0.08‰$ (standard error on the mean, $\sigma_{SEM} = \sigma_m/\sqrt{n}$) an offset of $+0.31 \pm \sigma_{diff} = 0.09‰$ (standard error on difference, $\sigma_{diff} = \sqrt{(\sigma_1^2 + \sigma_2^2)}$) from the nearest $\delta^{13}C_{DIC}$ measurement at WOCE station P06–215. Apparent offsets of similar magnitude have been described in other Southwest Pacific cores [*McCave et al.*, 2008]. However, in all these cases, in the absence of both core top material and more local $\delta^{13}C_{DIC}$ measurements, there is no clear basis for the application of a downcore offset.

[25] Two effects that have been documented to lead to a breakdown in the $\delta^{13}C_{DIC}$ to $\delta^{13}C_{benthic}$ relationship are carbonate dissolution and productivity overprints. The core site of MD06–3018 is not affected significantly by dissolution as it is situated ~600 m above the modern lysocline depth in the NCT [*Martinez*, 1994]. $\delta^{13}C_{benthic}$ measured in *C. wuellerstorfi* in modern or past environments with high overlying productivity has been shown to yield considerable negative excursions from $\delta^{13}C_{DIC}$ [*Mackensen et al.*, 1993]. While the SWSP is a fairly oligotrophic region there is an upwelling zone along the axis of the western New Caledonia barrier reef which stimulates significant variations in seasonal productivity [*Alory et al.*, 2006; *Henin and Cresswell*, 2005]. However, the core location of MD06–3018 is 60 km seaward of the reef and therefore unlikely to experience strong upwelling fluxes. The reproducibility of the $\delta^{13}C_{benthic}$ data is similar to that for $\delta^{18}O_{benthic}$, thus there is no empirical evidence for local phytodetrital effects [*Mackensen et al.*, 1993]. $\delta^{13}C_{benthic}$ in MD06–3018 is considered to provide a reliable record of past deep water $\delta^{13}C_{DIC}$ variability at 2500 m depth in the NCT. However, the term $\delta^{13}C$ is used to distinguish inferences made about past $\delta^{13}C_{DIC}$ based on $\delta^{13}C_{benthic}$ measurements from direct measurements of $\delta^{13}C_{DIC}$.

4.2. Glacial-Interglacial Variability in the Regional Deep Water Mixing Regime

[26] In the modern circulation regime, UCDW/NPDW from the Central Pacific Basin provides the dominant influence on the SWSP deep water mixing regime. The ultimate source of the majority of both the UCDW and NPDW in the open Pacific is the DWBC. All DWBC origin deep water should be isotopically lighter than that found in the DWBC itself because the longer a deep water mass remains out of contact with the surface ocean and atmosphere, the more isotopically depleted its $\delta^{13}C_{DIC}$ signature becomes due to the "aging effect." This effect arises through the progressive addition of remineralized organic carbon from the overlying water column and will vary in strength according to variations in both deep water flow rate and productivity regime. One constraint on the mixing regime independent of past changes in these factors is that when the difference in $\delta^{13}C$ values at ~2500 m depth between the deep waters of the NCT and the DWBC ($\Delta\delta^{13}C_{NCT\text{-}DWBC}$) is >0‰, the NCT $\delta^{13}C$ signal cannot be explained entirely from a DWBC origin. In the modern regime, where both the aging effect and the relative influence of DWBC origin water can be quantified, the value of $\Delta\delta^{13}C_{NCT\text{-}DWBC}$ from $\delta^{13}C_{DIC}$ measurements is $+0.02 \pm \sigma_{diff} = 0.04‰$ (Table 2). The positive value reflects the

Table 2. Terms Used in the Comparison of Regional $\delta^{13}C$ Records[a]

Term	Definition	Modern $\Delta\delta^{13}C_{DIC}$ (‰)	Late Holocene (0–5 ka) Value (‰)	Average Interglacial Stage Value, n = 39 (‰)	Average Glacial Stage Value, n = 35 (‰)	Difference in Average Interglacial-Glacial Stage Values (‰)	Student's *t* test Two-Tailed *p* Value for Interglacial-Glacial Difference
$\Delta\delta^{13}C_{MD06\text{-}ODP1123}$	Difference in $\delta^{13}C$ between core sites of MD06-3018 and ODP 1123	-0.17; $\pm\sigma_{diff} = 0.04$	-0.20; $\pm\sigma_{diff} = 0.11$	-0.08; $\pm\sigma_{SEM} = 0.04$; $\sigma = 0.20$	+0.48; $\pm\sigma_{SEM} = 0.04$; $\sigma = 0.24$	-0.56; $\pm\sigma_{diff} = 0.05$	$p < 0.0001$
$\Delta\delta^{13}C_{NCT\text{-}DWBC}$	Difference in $\delta^{13}C$ between 2500m in the NCT and the DWBC	+0.02; $\pm\sigma_{diff} = 0.04$	>-0.20; $\pm\sigma_{diff} = 0.11$	>-0.08; $\pm\sigma_{SEM} = 0.04$; $\sigma = 0.20$	>+0.48; $\pm\sigma_{SEM} = 0.04$; $\sigma = 0.24$	>-0.56; $\pm\sigma_{diff} = 0.05$	$p < 0.0001$
$\Delta\delta^{13}C_{MD06\text{-}ODP849}$	Difference in $\delta^{13}C$ between core sites of MD06-3018 and ODP 849	+0.25; $\pm\sigma_{diff} = 0.04$	+0.40; $\pm\sigma_{diff} = 0.12$	+0.37; $\pm\sigma_{SEM} = 0.04$; $\sigma = 0.11$	+0.33; $\pm\sigma_{SEM} = 0.04$; $\sigma = 0.15$	+0.04; $\pm\sigma_{diff} = 0.03$	$p = 0.16$
$\Delta\delta^{13}C_{NCT\text{-}CPBDW}$	Difference in $\delta^{13}C$ between 2500m in the NCT and the Central Pacific Basin	+0.13; $\pm\sigma_{diff} = 0.04$	>-0.20; $\pm\sigma_{diff} = 0.11$	>-0.09; $\pm\sigma_{SEM} = 0.04$; $\sigma = 0.19$	>+0.29; $\pm\sigma_{SEM} = 0.04$; $\sigma = 0.14$	>-0.38; $\pm\sigma_{diff} = 0.04$	$p < 0.0001$

[a]The WOCE stations used for calculating $\Delta\delta^{13}C_{DIC}$ values are P06–215 (for MD06–3018 and NCT), P06–168 (for ODP 1123 and DWBC), P18–163 (for ODP 849) and P14–165 (for CPBDW). The late Holocene $\Delta\delta^{13}C_{benthic}$ terms are calculated from the difference of the averages of all available, unsmoothed data in the 0–5 ka age range. Where > symbols are used, this indicates the use of $\Delta\delta^{13}C_{benthic}$ as an estimate of the minimum value of $\Delta\delta^{13}C$. The "n" values for the average interglacial and glacial columns refer to the number of data points used in each case. The error terms are defined in the text.

known Tasman Sea deep water influence but is within one standard deviation of zero, consistent with the known dominance of DWBC waters. To test whether this dominance persisted in the past, the MD06–3018 $\delta^{13}C_{benthic}$ record is compared to another record of similar age range from underneath the DWBC.

[27] ODP Site 1123 is located on the North Chatham Drift in the Southwest Pacific Basin at 3290 m depth [*Hall et al.*, 2001] (Figure 1 and Table 1). Before using the ODP 1123 $\delta^{13}C_{benthic}$ record to evaluate $\Delta\delta^{13}C_{NCT\text{-}DWBC}$ over the past 1.1 Ma it is first necessary to evaluate the assumptions involved in the comparison of the two records. The original age model for ODP 1123 is based on the SPECMAP timescale [*Imbrie and Imbrie*, 1980] and has been adjusted to that of MD06–3018 using the $\delta^{18}O_{benthic}$ records (Figure 6a) over the past 1.1 Ma. The sedimentation rate seen at the site of ODP 1123 is approximately twice that seen at MD06–3018, leading to a higher temporal sampling resolution and a reduced relative effect of bioturbation on the glacial-interglacial amplitudes in $\delta^{18}O_{benthic}$ and $\delta^{13}C_{benthic}$ at ODP 1123. In order to directly compare the stable isotope records, all records are smoothed to a 5 kyr resolution using linear interpolation around a moving average. The uncertainty in the age model correlation is dominated by this smoothing timescale.

[28] The ODP 1123 $\delta^{13}C_{benthic}$ measurements were made on infaunal *Uvigerina* taxa rather than the epibenthic *C. wuellerstorfi*. Due to their differing habitats the two groups may respond differently to changes in overlying productivity and organic carbon accumulation [*Zahn et al.*, 1986]. Furthermore, frontal movement on the glacial-interglacial timescale in the Southwest Pacific Basin have been shown to lead to significant variability in productivity at the site of ODP 1123 [*Crundwell et al.*, 2008]. Thus, we follow a transfer function method based on *Uvigerina* $\delta^{18}O_{benthic}$ to convert *Uvigerina* $\delta^{13}C_{benthic}$ measurements to *Cibicides*-equivalent rather than simply applying a constant offset [*McCave et al.*, 2008]. The transfer function is derived from coupled *Uvigerina* and *Cibicides* measurements from another core at similar latitude to ODP 1123 in the Southwest Pacific Basin [*McCave et al.*, 2008]. This approach generates more positive interglacial than glacial offsets between the two groups in response to the regional productivity changes. The late Holocene (0–5 ka) average *Cibicides*-equivalent $\delta^{13}C_{benthic}$ value (n = 5) using the transfer function is 0.76 ± σ_{SEM} = 0.07‰, an apparent offset of +0.34 ± σ_{diff} = 0.08‰ from $\delta^{13}C_{DIC}$ at 3300 m at WOCE station P06–168. The errors calculated here assume the same reproducibility error on individual $\delta^{13}C_{benthic}$ measurements as in MD06–3018 (σ_m = 0.16‰). The late Holocene offset from modern $\delta^{13}C_{DIC}$ is similar to that found for MD06–3018, suggesting that variability in the $\delta^{13}C_{DIC}$ gradient between the two sites may be reconstructed with greater confidence than the absolute value at either site alone.

[29] ODP 1123 is situated at ~800 m greater water depth than MD06–3018 (Figure 2). Although this means that ODP 1123 is closer to the modern regional lysocline depth than MD06–3018, shoaling of the lysocline to the depth of the ODP 1123 core site does not seem to have occurred over the past 1.2 Ma and glacial-interglacial differences in carbonate

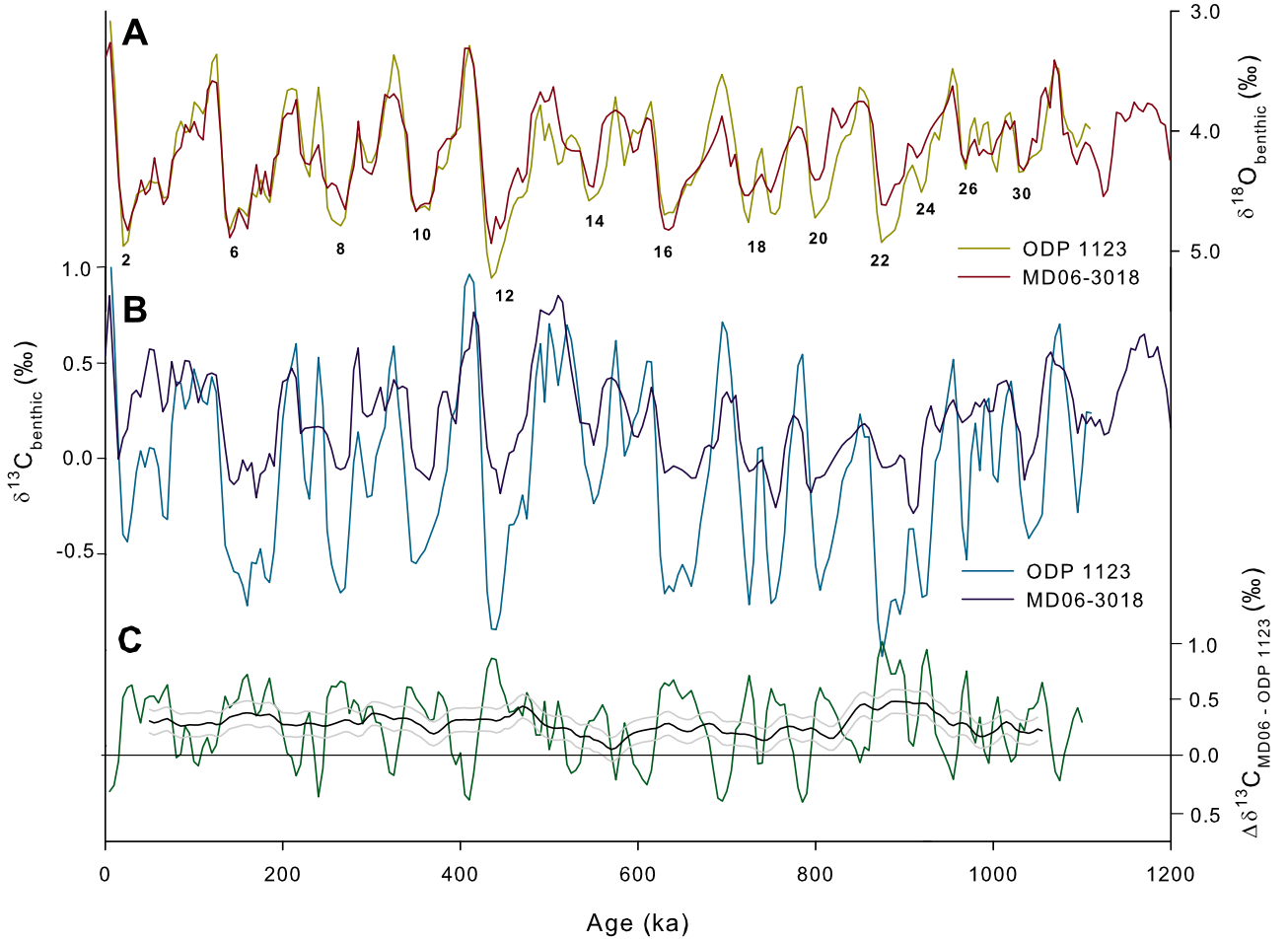

Figure 6. (a) Comparison of MD06–3018 $\delta^{18}O_{benthic}$ data with that from ODP 1123 to demonstrate adjustment of the age model to that of MD06–3018. The period from 1100 ka to the end of the record for ODP 1123 is not shown because of the difficulties in matching the age models in this interval. Numbers refer to selected glacial marine isotope stages. (b) Comparison of MD06–3018 $\delta^{13}C_{benthic}$ data with that from ODP 1123. (c) $\Delta\delta^{13}C_{MD06-ODP1123}$ and its 100 kyr moving average (black line) with 95% confidence intervals (gray lines).

dissolution are very small [*Crundwell et al.*, 2008]. The depth difference between the two cores does mean that the difference in $\delta^{13}C_{benthic}$ values ($\Delta\delta^{13}C_{MD06-ODP1123}$) cannot be used as a direct proxy for past $\Delta\delta^{13}C_{NCT-DWBC}$ unless the vertical gradient of $\delta^{13}C$ in the DWBC region is also known. Depth transect studies in the region have shown that the $\delta^{13}C$ values at 2500 m remain more negative than those at 3300 m over the past two glacial cycles [*McCave et al.*, 2008]. If it is assumed that this relationship holds across the past 1.1 Ma then the value of $\Delta\delta^{13}C_{MD06-ODP1123}$ provides an estimate of the minimum value of $\Delta\delta^{13}C_{NCT-DWBC}$ (Table 2). The criterion $\Delta\delta^{13}C_{MD06-ODP1123}$ >0‰ therefore provides an even more conservative estimate of when the influence of non-DWBC origin deep water on the mixing regime is required.

[30] Over the past 1.1 Ma the $\Delta\delta^{13}C_{MD06-ODP1123}$ record shows 10–100 kyr variability with amplitude of ~1‰ around a long-term mean value of 0.27‰ (Figure 6c). Given the errors arising from the alignment of the core age models and subsequent data smoothing, any given $\Delta\delta^{13}C_{MD06-ODP1123}$ value cannot be deemed diagnostic of conditions in that 5 kyr interval. However, the more positive excursions are seen to generally correspond with glacial periods and the more negative excursions with interglacial periods (Figure 7a). The average value of all the "interglacial" data points over the past 1.1 Ma, defined as those for which the corresponding MD06–3018 $\delta^{18}O_{benthic}$ data point lies within ±5 kyr of an interglacial $\delta^{18}O_{benthic}$ minimum and excluding those falling during a glacial termination, is $-0.08 \pm \sigma_{SEM} = 0.04$‰ with a one standard deviation spread on the data (σ) of 0.20‰ (Figure 7a and Table 2). The average value of the "glacial" points is $0.48 \pm \sigma_{SEM} = 0.04$‰ with $\sigma = 0.24$‰. The $\Delta\delta^{13}C_{MD06-ODP1123}$ data points constitute a broadly normally distributed population and thus, while the values of individual data points cannot be robustly compared, an unpaired student t test may be used to statistically determine whether the averaged interglacial and glacial stage values differ at a given confidence level. At the 95% confidence level (2σ), the p value for such a test is <0.0001, demon-

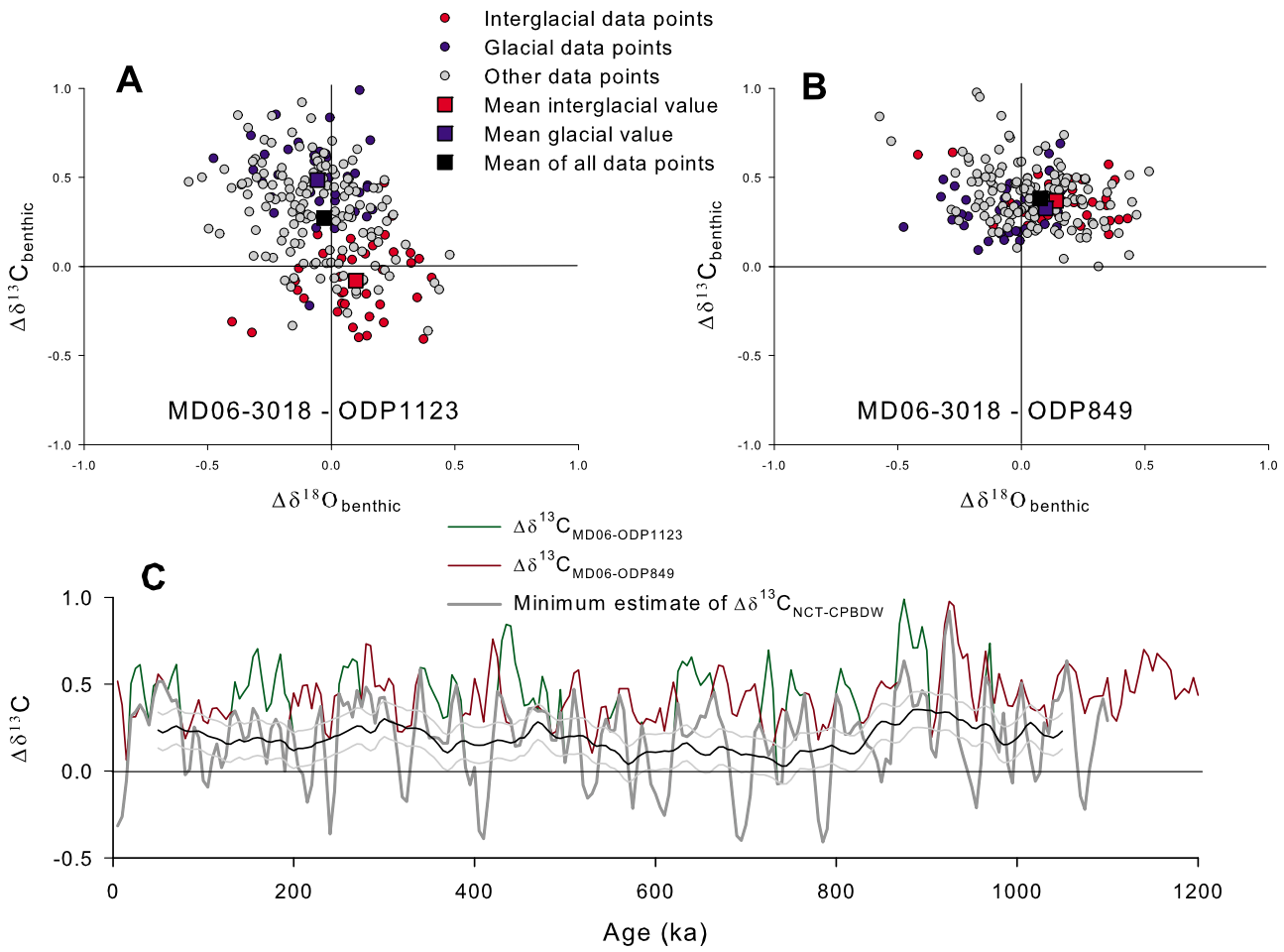

Figure 7. (a) $\Delta\delta^{13}C_{benthic}$ and $\Delta\delta^{18}O_{benthic}$ data for the MD06–3018 and ODP 1123 comparison. Data points are grouped by interglacial, glacial, or other stage (see text for definition used) and the average values for the interglacial, glacial, and complete data sets are shown. (b) $\Delta\delta^{13}C_{benthic}$ and $\Delta\delta^{18}O_{benthic}$ data for the MD06–3018 and ODP 849 comparison. (c) $\Delta\delta^{13}C_{MD06-OD1123}$ and $\Delta\delta^{13}C_{MD06-ODP849}$ plotted together to show the development of the composite minimum value estimate to $\Delta\delta^{13}C_{NCT-CPBDW}$. The 100 kyr moving average of the composite estimate is shown (black line) with 95% confidence intervals (gray lines).

strating that there is significant statistical difference in the average interglacial and glacial stage $\Delta\delta^{13}C_{MD06-ODP1123}$ gradients.

[31] The same exercise performed for the $\Delta\delta^{18}O_{MD06-ODP1123}$ values demonstrates an average interglacial value of $0.10 \pm \sigma_{SEM} = 0.03$‰ with $\sigma = 0.18$‰ and an average glacial value of $-0.05 \pm \sigma_{SEM} = 0.03$‰ with $\sigma = 0.16$‰ (Figure 7a). The offset between and nonzero value of the interglacial and glacial stage averages arises principally from the differential effects bioturbation in the two cores. The slower sedimentation rate at MD06–3018 leads to an average glacial-interglacial $\delta^{18}O_{benthic}$ amplitude which is ~90% of that at ODP 1123. This effect, while statistically significant ($p = 0.002$ at the 95% confidence interval) in itself, cannot account for the significance of the $\Delta\delta^{13}C_{MD06-ODP1123}$ offset. The interglacial-glacial $\Delta\delta^{18}O_{MD06-ODP1123}$ offset as a proportion of the glacial-interglacial variability in the ODP 1123 record is only ~10% whereas for $\Delta\delta^{13}C_{MD06-ODP1123}$ it is ~50%.

[32] The late Holocene value of $\Delta\delta^{13}C_{MD06-ODP1123}$ does not significantly differ (at the 1σ level) from the average interglacial stage value (Table 2). If it is assumed that the vertical $\delta^{13}C$ profile, deep water flow rate and overlying productivity regime in the DWBC and SWSP were similar to the modern during past interglacial stages then it follows that the modern mixing regime, in which DWBC origin deep waters dominate but a small influence from Tasman Sea deep waters also exists, is representative of average interglacial conditions over the past 1.1 Ma. If these assumptions are not made, then at the minimum estimate, under average interglacial conditions NCT $\delta^{13}C$ can be explained entirely from a DWBC origin. The same assumptions are definitely not justified under glacial conditions. However, even at the minimum estimate, the average glacial stage $\Delta\delta^{13}C_{MD06-ODP1123}$ value is significantly more positive than not only the average interglacial stage value but also the modern $\Delta\delta^{13}C_{NCT-DWBC}$ value. Thus, during glacial conditions the influence on the SWSP mixing regime

required from a water mass chemically younger than that found at 2500 m in the DWBC was significantly enhanced compared to both the modern regime and likely past interglacial conditions. This could arise from the enhanced relative influence of glacial Tasman Sea deep waters (affecting arrow B on Figure 1) and/or the presence of an additional chemically younger water mass in the glacial Central Pacific Basin (affecting arrow A on Figure 1).

4.2.1. Glacial Decoupling of DWBC to Central Pacific Basin Deep Waters

[33] The $\delta^{13}C_{benthic}$ gradient between ODP 1123 and ODP 849 [*Mix et al.*, 1995] from 3840 m water depth on the East Pacific Rise (Figure 1 and Table 1) decreases significantly (and even reverses in certain stages) during past glacials [*Hall et al.*, 2001]. This means that the $\delta^{13}C$ of glacial deep waters in the equatorial Pacific can no longer be readily explained simply as more chemically aged DWBC waters [*McCave et al.*, 2008]. One hypothesis to explain this change is the presence of a chemically younger water mass resulting from the ventilation of deep waters in the glacial North Pacific [*Keigwin*, 1998; *Matsumoto et al.*, 2001]. If the chemical signature of such water penetrates far enough south to influence the southern Central Pacific Basin and enter the SWSP, it could potentially account for the very positive glacial stage $\Delta\delta^{13}C_{NCT-DWBC}$ values without any need for changes in the relative influence from Tasman Sea deep waters.

[34] To constrain the potential effect of such open Pacific circulation changes on the SWSP mixing regime it is assumed that the $\delta^{13}C$ values of deep waters at 2500 m depth in the southern Central Pacific Basin ($\delta^{13}C_{CPBDW}$) can always be explained from an admixture of DWBC and equatorial Pacific deep waters at that depth. The minimum relative contribution to the observed NCT $\delta^{13}C$ values required from nonopen Pacific deep waters can then be evaluated from $\Delta\delta^{13}C_{NCT-CPBDW}$ rather than $\Delta\delta^{13}C_{NCT-DWBC.}$ Considering the aging effect, it follows that the chemistry of open Pacific Ocean deep waters cannot account for all NCT $\delta^{13}C$ variability in the case that $\Delta\delta^{13}C_{NCT-CPBDW} > 0‰$.

[35] ODP Site 806B [*Berger et al.*, 1996; *Bickert et al.*, 1993] provides a record of $\delta^{13}C_{benthic}$ over the past ~750 ka from the western equatorial Pacific at 2520 m depth (Figure 1 and Table 1). In the modern regime, the site of ODP 806B is bathed by NPDW and should record the signature of any glacial North Pacific origin deep waters that could possibly reach further south into the SWSP. At equatorial latitudes in the modern Pacific, the mixing of NPDW and CDW is zonally homogenous [*Reid*, 1997] such that the longer ODP 849 record from the deep eastern equatorial Pacific allows the comparison to be extended back to 1500 ka. Throughout the ODP 806B record the two equatorial $\delta^{13}C_{benthic}$ records are strongly correlated (Figure 8b) suggesting that the depth difference between the sites does not lead to a significant difference in isotopic composition. The ODP 806B $\delta^{13}C_{benthic}$ measurements are made entirely on *C. wuellerstorfi* and the ODP 849 ones predominantly so, with some *Uvigerina* measurements that have been corrected to *Cibicides*-equivalent using a constant offset. Both records are compared directly to the MD06–3018 $\delta^{13}C_{benthic}$ (Figure 8b) values after correlation of the age models (Figure 8a). Sedimentation rates at both equatorial sites are closer to that seen at MD06–3018 than was the case for ODP 1123. Thus, the degree of glacial-interglacial smoothing of $\delta^{18}O_{benthic}$ and $\delta^{13}C_{benthic}$ values is similar and the difference between the average interglacial and glacial stage $\Delta\delta^{18}O_{MD06-ODP849}$ values is less than 0.05‰ (Figure 7b).

[36] Across the past 1.1 Ma, the $\Delta\delta^{13}C_{MD06-ODP849}$ record shows a long-term mean of 0.38‰ and generally lower-amplitude 10–100 kyr variability than that seen in $\Delta\delta^{13}C_{MD06-ODP1123}$ (Figure 8c). The average interglacial value over the past 1.1 Ma for $\Delta\delta^{13}C_{MD06-ODP849}$ is 0.37 ± σ_{SEM} = 0.04‰ with σ = 0.11‰ and the average glacial value is 0.33 ± σ_{SEM} = 0.04‰ with σ = 0.15‰ (Figure 7b and Table 2). These populations show no significant statistical difference at the 95% level (p = 0.16) using the student t test method. Thus, whereas the $\Delta\delta^{13}C_{MD06-ODP1123}$ record shows significant glacial-interglacial variability caused by changes in deep water chemistry and/or circulation, the uniformity of offset seen in the $\Delta\delta^{13}C_{MD06-ODP849}$ record suggests that the amplitude of glacial-interglacial $\delta^{13}C$ variability at both sites is dominated by global mean ocean chemistry changes.

[37] The value of $\Delta\delta^{13}C_{NCT-CPBDW}$ must lie between those of $\Delta\delta^{13}C_{MD06-ODP849}$ and $\Delta\delta^{13}C_{MD06-ODP1123}$. The least positive possible estimate of $\Delta\delta^{13}C_{NCT-CPBDW}$ over the past 1.1 Ma may thus be derived from a composite of the two records (Figure 7c). The average interglacial stage value over the past 1.1 Ma for this minimum estimate to $\Delta\delta^{13}C_{NCT-CPBDW}$ is −0.09 ± σ_{SEM} = 0.04‰ with σ = 0.19‰ and the average glacial value is 0.29 ± σ_{SEM} = 0.04‰ with σ = 0.14‰ (Table 2). At the 95% confidence level (2σ), the p value for a student t test of these two populations is 0.006. Even when the potential ventilation of North Pacific Deep Water is considered, it remains the case that open Pacific deep waters can potentially explain NCT $\delta^{13}C$ values under interglacial conditions but cannot do so under glacial conditions. The most plausible explanation is that the relative influence on the mixing regime from Tasman Sea deep waters was significantly enhanced during glacial in comparison to interglacial stages.

4.2.2. Glacial Stage Deep Water Chemistry Gradients in the Southwest Pacific

[38] Changes in either the relative fluxes or $\delta^{13}C_{DIC}$ values associated with the Tasman Sea and open Pacific Ocean inflows to the SWSP region could account for the observed glacial-interglacial variability in the mixing regime. Pleistocene reconstructions of DWBC flow strength at site ODP 1123 have shown generally increased fluxes during glacial stages [*Hall et al.*, 2001]. This suggests that the relatively reduced DWBC influence seen in the glacial SWSP cannot be explained by flow rate changes in the DWBC. In the absence of reconstructions for the past inflow rates from the Tasman Sea it remains impossible to quantitatively reconstruct the mixing regime. However, given the assumption that NCT $\delta^{13}C$ values arise from a mixture of only open Pacific Ocean and Tasman Sea deep waters, the MD06–3018 $\delta^{13}C_{benthic}$ record may be used to place a constraint on the $\delta^{13}C$ values of northern Tasman

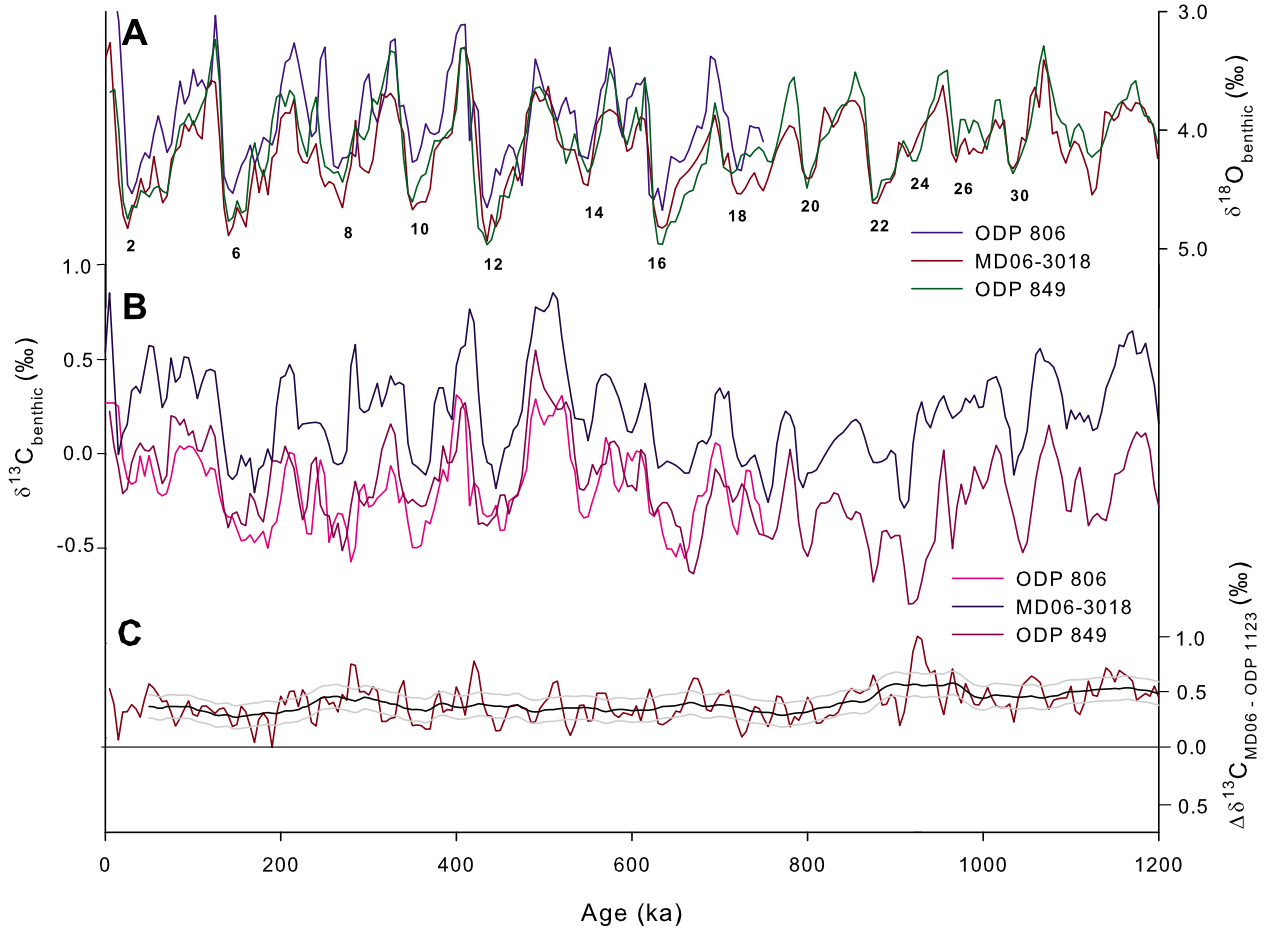

Figure 8. (a) Comparison of MD06–3018 $\delta^{13}C_{benthic}$ data with that from ODP 806B and ODP 849 to demonstrate adjustment of the age models to that of MD06–3018. (b) Comparison of MD06–3018 $\delta^{13}C_{benthic}$ data with that from ODP 806B and ODP 849. (c) $\Delta\delta^{13}C_{MD06-ODP849}$ and its 100 kyr moving average (black line) with 95% confidence intervals (gray lines).

Sea deep water at ~2500 m depth. In periods where some influence from Tasman Sea deep water is required (those during which the minimum value of $\Delta\delta^{13}C_{NCT-CPBDW}$ is >0‰) the $\delta^{13}C$ value of this water mass must be more positive than the corresponding MD06–3018 $\delta^{13}C_{benthic}$ value.

[39] During the last two glacial stages (the LGM and MIS 6) in the DWBC region, isotopically depleted ($\delta^{13}C$ values of <−0.5‰) Southern Ocean sourced Glacial Upper Circumpolar Deep Water (gUCDW) replaced NPDW/UCDW as the dominant water mass in the "middle-depth" range 2000–3500 m [*McCave et al.*, 2008]. In contrast, the MD06–3018 constraint on $\delta^{13}C$ at ~2500 m depth in the northern Tasman Sea suggests average glacial stage $\delta^{13}C$ values of >0.2‰. This suggests that the gUCDW present in the DWBC region [*McCave et al.*, 2008] was not present as the dominant middle-depth water mass in the glacial Tasman Sea.

[40] The modern $\delta^{13}C$–depth gradient across the range 2500–3500 m in the Tasman Sea is close to zero (Figure 2c, station P06–234). The MD97–2106 $\delta^{13}C_{benthic}$ record from 3310 m water depth on the South Tasman Rise, where most deep water enters the Tasman Sea from the Southern Ocean (Figure 1 and Table 1), shows average values of −0.25‰ during the LGM and −0.40‰ during MIS 6 [*Moy et al.*, 2006]. These values are slightly more positive than those seen in the glacial DWBC but still significantly more negative than those predicted for 2500 m in the average glacial stage northern Tasman Sea. Therefore, during at least the past two glacial stages the $\delta^{13}C$–depth gradient in the Tasman Sea became significantly negative, consistent with the presence of a glacial stage chemocline at 2500–3000 m depth. In contrast, the glacial DWBC $\delta^{13}C$–depth gradient retained the modern positive value over the same depth range [*McCave et al.*, 2008]. The future study of a Pleistocene $\delta^{13}C$ record from ~2500 m depth in the northern Tasman Sea will allow direct evaluation of this hypothesis.

[41] At depths below ~3500 m several deep hydrographic zones with different characteristic $\delta^{13}C$ signatures have been proposed for glacial Southern Ocean bottom waters [*McCave et al.*, 2008; *Ninnemann and Charles*, 2002]. In one scenario the bottom waters flowing into the southern Atlantic sector are formed in the Weddell Sea, those entering the open Pacific in the Ross Sea and those entering

the Tasman Sea along the Adélie Coast [*McCave et al.*, 2008]. The SWSP mixing constraint additionally demonstrates that the $\delta^{13}C$ gradient between Tasman Sea and DWBC waters at ~2500 m was significantly enhanced during glacial over interglacial stages.

[42] The enhanced glacial stage spatial $\delta^{13}C$ gradient could be explained if the isotopically enriched water of North Atlantic origin which lies at or above the observed glacial-stage chemocline at 2100–2700 m in the southern Atlantic sector of the Southern Ocean [*Hodell et al.*, 2003; *Ninnemann and Charles*, 2002; *Venz and Hodell*, 2002] was able to pass round the glacial Circumpolar Current and enter the Tasman Sea but not the Pacific DWBC. Alternatively, the middle-depth glacial Tasman Sea could be filled with Southern Ocean sourced deep water, but this water mass would be required to be isotopically enriched in relation to the gUCDW seen in the DWBC. Therefore, in addition to the previously described threefold zonation of glacial Southern Ocean bottom waters [*McCave et al.*, 2008], a strong spatial chemical gradient existed between the overlying middle-depth waters associated with the Adélie Coast and Ross Sea bottom water domains but apparently not between those of the Weddell Sea and Adélie Coast domains.

[43] The existence of strong vertical and spatial $\delta^{13}C$ gradients in the deep glacial Southern Ocean has important implications for the glacial-interglacial carbon cycle. Reconstructions of the vertical deep water $\delta^{13}C$ gradient in the southern Atlantic sector of the Southern Ocean resembles the variability seen in the Vostok atmospheric pCO_2 record [*Hodell et al.*, 2003]. This provides empirical support to modeling studies suggesting that an enhanced stratification of the glacial deep ocean can significantly contribute to lowering atmospheric pCO_2 [*Toggweiler*, 1999]. However, the picture is made more complex as the glacial Southern Ocean is increasingly seen to also show strong spatial heterogeneity at all depths below ~2000 m. Specifically, the glacial chemocline seen in the southern Atlantic sector is shown to extend as far east as the Tasman Sea, but not into the southern Pacific sector. This is consistent with the presence of highly depleted glacial $\delta^{13}C_{benthic}$ values seen in cores below ~2500 m depth being restricted to the southern Atlantic and Indian Ocean sectors [*Hodell et al.*, 2003]. The absence of similar stratification in the southern Pacific sector necessarily limits the volume of deep water available for enhanced glacial storage of atmospheric carbon in the deep Southern Ocean.

4.3. Middle-Late Pleistocene Evolution of Deep Water Circulation and Mixing

[44] As well as glacial-interglacial variability, all of the $\delta^{13}C_{benthic}$ records discussed here show a perturbation toward more negative mean values during the period of the MPT (Figures 6b and 8b). This perturbation is also recorded in all other major ocean basins and has been interpreted as a global shift in mean ocean $\delta^{13}C$ [*Raymo et al.*, 1997]. In this global average, the perturbation constitutes a decrease in mean ocean $\delta^{13}C$ of ~0.3‰ during the period 1000–900 ka followed by a more gradual return to pre-1000 ka values by 400 ka [*Raymo et al.*, 1997].

[45] To study the behavior of the SWSP deep water mixing regime on these longer timescales the effect of glacial-interglacial variability is removed by considering the running mean value (100 kyr linear smoothing using a boxcar method) of $\Delta\delta^{13}C_{NCT\text{-}CPBDW}$ (Figure 7c). The values of this minimum estimate are almost always positive (at the 2σ level), demonstrating that on this timescale there is always a component of variability in SWSP deep water $\delta^{13}C$ that cannot be explained by the influence of open Pacific Ocean deep waters alone. However, the value of the running mean $\Delta\delta^{13}C_{NCT-CPDW}$ varies across the past 1.1 Ma, indicating long-term shifts in the mode of the deep water circulation regime.

[46] In the period 500–0 ka the mean value for the estimate of the minimum value of $\Delta\delta^{13}C_{NCT-\ CPBDW}$ was 0.20‰, whereas during the period 1100–900 ka it was 0.24‰. In the intervening period, the mean value decreased by 0.32‰ during the interval 900–750 ka and then generally increased across the interval 750–500 ka during which the mean value was 0.11‰. The spatial gradient between deep waters entering the Pacific DWBC and Tasman Sea from the Southern Ocean was, therefore, decreased during the period 900–500 ka, coincident with the main part of the global mean ocean $\delta^{13}C$ perturbation across the MPT.

[47] The MPT is associated with generally weaker global deep water exchange [*Schmieder et al.*, 2000]. Reconstructions of the flow strength associated with water masses in the Pacific DWBC suggest reduced flow during the period 900–400 ka [*Hall et al.*, 2001; *Venuti et al.*, 2007]. Because the majority of northward flow in the DWBC is of Southern Ocean origin deep and bottom waters, this may represent reduced ventilation of the Southern Ocean over this period. Furthermore, the ventilation of North Atlantic deep waters is also thought to be reduced across the MPT [*Raymo et al.*, 1997]. The MD06–3018 $\delta^{13}C_{benthic}$ record is more sensitive to changes in the ventilation rates of North Atlantic deep waters than the ODP 1123 and ODP 849 $\delta^{13}C_{benthic}$ records. This arises because the SWSP deep water mixing regime means that NCT deep water is sensitive to both DWBC and Tasman Sea deep water chemistry whereas open Pacific Ocean deep water is sensitive mainly to the former. Middle-depth deep waters in the Tasman Sea show more influence from relict North Atlantic deep waters than those of the DWBC and this difference is shown to be enhanced during past glacial stages. Therefore, a reduction in the ventilation of both North Atlantic and Southern Ocean deep waters could lead to the observed reduction in the $\delta^{13}C$ gradient between the middle-depth waters of the Tasman Sea and DWBC during the MPT.

5. Conclusions

[48] The modern deep water $\delta^{13}C_{DIC}$ distribution in the SWSP region is consistent to the first order with conservative water mass properties and the modern deep water mixing regime between open Pacific Ocean and Tasman Sea sourced deep waters [*Wyrtki*, 1961]. A reconstruction of deep water $\delta^{13}C$ in the NCT, in comparison with other regional records allows constraints to be placed on aspects of the mixing regime across the middle-late Pleistocene.

[49] On the glacial-interglacial timescale the difference in $\delta^{13}C_{benthic}$ values between the NCT record and a core from the Pacific DWBC shows a significantly more positive value during glacial than interglacial stages. The effect of potential ventilation of deep waters in the North Pacific on this offset is examined using the comparison of the NCT $\delta^{13}C_{benthic}$ record with ones from the deep equatorial Pacific. Even with these possible circulation changes, glacial stage NCT $\delta^{13}C$ values cannot be explained entirely from a purely open Pacific Ocean source. Instead, a significantly enhanced relative influence from glacial Tasman Sea deep waters compared to those from the open Pacific is required in comparison to the interglacial regime. The enhanced relative influence of Tasman Sea over open Pacific deep waters during glacial stages reflects a steepening of the spatial gradient between the $\delta^{13}C$ of deep waters found at ~2500 m depth in the Tasman Sea and the Pacific DWBC. This arose from the relatively greater glacial stage influence of isotopically depleted middle-depth waters of Southern Ocean origin in the DWBC compared to the Tasman Sea. The glacial stage Southern Ocean is shown to contain significant spatial chemical gradients at depths well above the seafloor topography. Such regionalization has important implications for the overall storage capacity of the deep Southern Ocean as a reservoir for glacial stage carbon.

[50] On the >100 kyr timescale the influence of the chemically younger Tasman Sea deep waters on the mixing regime is seen to be a persistent feature of the past 1.1 Ma. The spatial $\delta^{13}C$ gradient between the middle-depth deep waters of the Tasman Sea and the Pacific DWBC was generally reduced during the period of the MPT, consistent with this being a period of reduced deep water ventilation in both hemispheres.

[51] **Acknowledgments.** Colin Chilcott is thanked for assistance with the mass spectrometer. Denis Wirrmann and Anne-Marie Sémah (IRD, UMR LOCEAN) and the other crew and scientists from IPEV on board the RV *Marion Dufresne*, particularly Yvon Balut, are thanked for their participation during the cruise. Yves Lafoy (Service de la Géologie de Nouvelle Calédonie, Direction de l'industrie, des mines et de l'énergie) is thanked for the invitation to share the cruise. Our thanks are also extended to the French ZONECO program which granted the cruise AUSFAIR/ZoNéCo 12. Helen Bostock is thanked for productive discussions of the project. Reviews from Gavin Dunbar and an anonymous reviewer greatly improved the manuscript. This work was funded through NERC Ph.D. studentship 14325 to T. Russon. The magnetic measurements were made at the LSCE in France with the help of C. Wandres and funds from the Commissariat à l'Energie Atomique and the Centre National de la Recherche Scientifique.

References

Alory, G., A. Vega, A. Ganachaud, and M. Despinoy (2006), Influence of upwelling, subsurface stratification, and heat fluxes on coastal sea surface temperature off southwestern New Caledonia, *J. Geophys. Res.*, *111*(C7), C07023, doi:10.1029/2005JC003401.

Archer, D., A. Winguth, D. Lea, and N. Mahowald (2000), What caused the glacial/interglacial atmospheric pCO_2 cycles?, *Rev. Geophys.*, *38*(2), 159–189, doi:10.1029/1999RG000066.

Berger, W., and E. Jansen (1994), Mid-Pleistocene climate shift: The Nansen Connection, in *The Polar Oceans and Their Role in Shaping the Global Environment*, edited by O. M. Johannessen et al., pp. 295–313, AGU, Washington D. C.

Berger, W. H., T. Bickert, M. K. Yasuda, and G. Wefer (1996), Reconstruction of atmospheric CO_2 from ice-core data and the deep-sea record of Ontong Java plateau: The Milankovitch chron, *Geol. Rundsch.*, *85*, 466–495, doi:10.1007/BF02369003.

Bickert, T., W. H. Berger, S. Burke, H. Schmidt, and G. Wefer (1993), Late Quaternary stable isotope record of benthic foraminifers: Sites 805 and 806, Ontong Java plateau, *Proc. Ocean Drill. Program Sci. Results*, *130*, 411–420.

Bostock, H. C., B. N. Opdyke, M. K. Gagan, A. E. Kiss, and L. K. Fifield (2006), Glacial/interglacial changes in the East Australian Current, *Clim. Dyn.*, *26*, 645–659, doi:10.1007/s00382-005-0103-7.

Cande, S. C., and D. V. Kent (1995), Revised calibration of the geomagnetic polarity timescale for the Late Cretaceous and Cenozoic, *J. Geophys. Res.*, *100*(B4), 6093–6095, doi:10.1029/94JB03098.

Charles, C. D., and R. G. Fairbanks (1992), Evidence from Southern Ocean sediments for the effect of North Atlantic deep water flux on climate, *Nature*, *355*(6359), 416–419, doi:10.1038/355416a0.

Crowley, T. J. (1995), Ice-age terrestrial carbon changes revisited, *Global Biogeochem. Cycles*, *9*(3), 377–389, doi:10.1029/95GB01107.

Crundwell, M., G. Scott, T. Naish, and L. Carter (2008), Glacial-interglacial ocean climate variability from planktonic foraminifera during the Mid-Pleistocene transition in the temperate southwest Pacific, ODP Site 1123, *Palaeogeogr. Palaeoclimatol. Palaeoecol.*, *260*(1–2), 202–229, doi:10.1016/j.palaeo.2007.08.023.

Curry, W. B., and G. P. Lohmann (1982), Carbon isotopic changes in benthic foraminifera from the western South Atlantic: Reconstruction of glacial abyssal circulation patterns, *Quat. Res.*, *18*(2), 218–235, doi:10.1016/0033-5894(82)90071-0.

Curry, W. B., J.-C. Duplessy, L. Labeyrie, and N. J. Shackleton (1988), Changes in the distribution of $\delta^{13}C$ of deep water $SumCO_2$ between the last glaciation and the Holocene, *Paleoceanography*, *3*, 317–341, doi:10.1029/PA003i003p00317.

Duplessy, J. C., N. J. Shackleton, R. K. Matthews, W. Prell, W. F. Ruddiman, M. Caralp, and C. H. Hendy (1984), ^{13}C record of benthic foraminifera in the last interglacial ocean - Implications for the carbon-cycle and the global deep water circulation, *Quat. Res.*, *21*(2), 225–243, doi:10.1016/0033-5894(84)90099-1.

Duplessy, J. C., N. J. Shackleton, R. G. Fairbanks, L. Labeyrie, D. W. Oppo, and N. Kallel (1988), Deepwater source variations during the last climatic cycle and their impact on the global deepwater circulation, *Paleoceanography*, *3*, 343–360, doi:10.1029/PA003i003p00343.

Elliot, M., L. Labeyrie, and J. C. Duplessy (2002), Changes in North Atlantic deep-water formation associated with the Dansgaard-Oeschger temperature oscillations (60–10 ka), *Quat. Sci. Rev.*, *21*(10), 1153–1165, doi:10.1016/S0277-3791(01)00137-8.

Foucher, J. P., J. L. Charlou, F. Harmegnies, D. Wirrmann, A. M. Sémah, C. Chaduteau, and E. Roussel (2006), Rapport des travaux de la campagne ZoNéCo 12, Campagne AUSFAIR/ZoNéCo 12 à bord du N/O Marion Dufresne (12 au 26 février 2006), technical report, Inst. Fr. de Rech. pour l'Exploit. de la Mer, Issy-les-Moulineaux, France.

Gordon, A. L. (1975), An Antarctic oceanographic section along 170E, *Deep Sea Res., Oceanogr. Abstr.*, *22*, 357–377.

Gourdeau, L., W. S. Kessler, R. E. Davis, J. Sherman, C. Maes, and E. Kestenare (2008), Zonal jets entering the Coral Sea, *J. Phys. Oceanogr.*, *38*(3), 715–725, doi:10.1175/2007JPO3780.1.

Hall, I. R., I. N. McCave, N. J. Shackleton, G. P. Weedon, and S. E. Harris (2001), Intensified deep Pacfic inflow and ventilation in Pleistocene glacial times, *Nature*, *412*(6849), 809–812, doi:10.1038/35090552.

Harris, S. E. (2002), Data report: Late Pliocene-Pleistocene carbon and oxygen stable isotopes from benthic foraminifers at Ocean Drilling Program Site 1123 in the southwest Pacific, *Proc. Ocean Drill. Program Sci. Results*, *181*, 1–20, doi:10.2973/odp.proc.sr.181.203.2002.

Head, M. J., and P. L. Gibbard (2005), Early middle Pleistocene transitions: An overview and recommendation for the defining boundary, in *Early Middle Pleistocene Transitions: The Land-Ocean Evidence*, edited by M. J. Head and P. L. Gibbard, pp. 1–18, Geol. Soc., Bath, U. K.

Henin, C., and G. R. Cresswell (2005), Upwelling along the western barrier reef of New Caledonia, *Mar. Freshwater Res.*, *56*(7), 1005–1010, doi:10.1071/MF04266.

Hodell, D. A., K. A. Venz, C. D. Charles, and U. S. Ninnemann (2003), Pleistocene vertical carbon isotope and carbonate gradients in the South Atlantic sector of the Southern Ocean, *Geochem. Geophys. Geosyst.*, *4*(1), 1004, doi:10.1029/2002GC000367.

Imbrie, J., and J. Z. Imbrie (1980), Modeling the climatic response to orbital variations, *Science*,

207(4434), 943–953, doi:10.1126/science.207.4434.943.

Johnson, G. C., P. E. Robbins, and G. E. Hufford (2001), Systematic adjustments of hydrographic sections for internal consistency, *J. Atmos. Oceanic Technol.*, *18*(7), 1234–1244, doi:10.1175/1520-0426(2001)018<1234:SAOHSF>2.0.CO;2.

Keigwin, L. D. (1998), Glacial-age hydrography of the far northwest Pacific Ocean, *Paleoceanography*, *13*, 323–339, doi:10.1029/98PA00874.

Key, R. M., A. Kozyr, C. L. Sabine, K. Lee, R. Wanninkhof, J. L. Bullister, R. A. Feely, F. J. Millero, C. Mordy, and T. H. Peng (2004), A global ocean carbon climatology: Results from Global Data Analysis Project (GLODAP), *Global Biogeochem. Cycles*, *18*(4), GB4031, doi:10.1029/2004GB002247.

Kroopnick, P. M. (1985), The distribution of ^{13}C of ΣCO_2 in the world oceans, *Deep Sea Res., Part A*, *32*(1), 57–84, doi:10.1016/0198-0149(85)90017-2.

Lafoy, Y., I. Brodien, R. Vially, and N. F. Exon (2005), Structure of the basin and ridge system west of New Caledonia (southwest Pacific): A synthesis, *Mar. Geophys. Res.*, *26*(1), 37–50, doi:10.1007/s11001-005-5184-5.

Laj, C., and J. E. T. Channell (2007), Geomagnetic excursions, in *Geomagnatism*, edited by M. Kono, pp. 373–416, Elsevier, New York.

Lisiecki, L. E., and M. E. Raymo (2005), A Pliocene-Pleistocene stack of 57 globally distributed benthic delta O-18 records, *Paleoceanography*, *20*, PA1003, doi:10.1029/2004PA001071.

Maasch, K. A., and B. Saltzman (1990), A low-order dynamic-model of global climatic variability over the full Pleistocene, *J. Geophys. Res.*, *95*(D2), 1955–1963, doi:10.1029/JD095iD02p01955.

Mackensen, A., H. W. Hubberten, T. Bickert, G. Fischer, and D. K. Futterer (1993), The $\delta^{13}C$ in benthic foraminiferal tests of Fontbotia-*wuellerstorfi* (Schwager) relative to the $\delta^{13}C$ of dissolved inorganic carbon in Southern Ocean deep water: Implications for Glacial Ocean Circulation Models, *Paleoceanography*, *8*, 587–610, doi:10.1029/93PA01291.

Martinez, J. I. (1994), Late Pleistocene paleoceanography of the Tasman Sea: Implications for the dynamics of the warm pool in the western Pacific, *Palaeogeogr. Palaeoclimatol. Palaeoecol.*, *112*(1–2), 19–62, doi:10.1016/0031-0182(94)90133-3.

Matsumoto, K., J. Lynch-Stieglitz, and R. F. Anderson (2001), Similar glacial and Holocene Southern Ocean hydrography, *Paleoceanography*, *16*, 445–454, doi:10.1029/2000PA000549.

Mazaud, A. (2005), User-friendly software for vector analysis of the magnetization of long sediment cores, *Geochem. Geophys. Geosyst.*, *6*, Q12006, doi:10.1029/2005GC001036.

McCave, I. N., L. Carter, and I. R. Hall (2008), Glacial-interglacial changes in water mass structure and flow in the SW Pacific Ocean, *Quat. Sci. Rev.*, *27*, 1886–1908, doi:10.1016/j.quascirev.2008.07.010.

McCorkle, D. C., and L. D. Keigwin (1994), Depth profiles of $\delta^{13}C$ in bottom water and core top *C. wuellerstorfi* on the Ontong Java plateau and Emperor Seamounts, *Paleoceanography*, *9*, 197–208, doi:10.1029/93PA03271.

McTaggart, K. E., and G. C. Johnson (1997), CTD/O_2 measurements collected on a climate and global change cruise (WOCE Sections P14S and P15S) during January-March, 1996, *Data Rep. ERL PMEL-63 (NTIS PB98–110158)*, NOAA, 485 pp.

McTaggart, K. E., G. C. Johnson, and B. A. Taft (1994), CTD/O_2 measurements collected on a climate and global change cruise (WOCE section P13) along 165E during August-October, 1992, *Data Rep. ERL PMEL-51*, NOAA, 244 pp.

Michel, E., L. D. Labeyrie, J. C. Duplessy, N. Gorfti, M. Labracherie, and J. L. Turon (1995), Could deep sub-Antarctic convection feed the world deep basins during the last glacial maximum?, *Paleoceanography*, *10*, 927–941, doi:10.1029/95PA00978.

Mix, A. C., N. G. Pisias, W. Rugh, J. Wilson, A. Morey, and T. Hagelberg (1995), Benthic foraminiferal stable isotope record from site 849, 0–5 Ma: Local and global climate changes, *Proc. Ocean Drill. Program Sci. Results*, *138*, 371–412.

Moy, A. D., W. R. Howard, and M. K. Gagan (2006), Late Quaternary palaeoceanography of the circumpolar deep water from the South Tasman Rise, *J. Quat. Sci.*, *21*(7), 763–777, doi:10.1002/jqs.1067.

Mudelsee, M., and K. Stattegger (1997), Exploring the structure of the mid-Pleistocene revolution with advanced methods of time-series analysis, *Geol. Rundsch.*, *86*, 499–511, doi:10.1007/s005310050157.

Ninnemann, U. S., and C. D. Charles (2002), Changes in the mode of Southern Ocean circulation over the last glacial cycle revealed by foraminiferal stable isotopic variability, *Earth Planet. Sci. Lett.*, *201*(2), 383–396, doi:10.1016/S0012-821X(02)00708-2.

Pahnke, K., and R. Zahn (2005), Southern hemisphere water mass conversion linked with North Atlantic climate variability, *Science*, *307*(5716), 1741–1746, doi:10.1126/science.1102163.

Paillard, D., L. Labeyrie, and P. Yiou (1996), Macintosh program performs time-series analysis, *Eos Trans. AGU*, *77*(39), 379, doi:10.1029/96EO00259.

Pelletier, B. (2006), Geology of the New Caledonia region and its implications for the study of the New Caledonian biodiversity, paper presented at Forum Biodiversité des Ecosystèmes Coralliens, Nouméa, New Caledonia.

Piotrowski, A. M., S. L. Goldstein, S. R. Hemming, and R. G. Fairbanks (2005), Temporal relationships of carbon cycling and ocean circulation at glacial boundaries, *Science*, *307*(5717), 1933–1938, doi:10.1126/science.1104883.

Raymo, M. E., D. W. Oppo, and W. Curry (1997), The mid-Pleistocene climate transition: A deep sea carbon isotopic perspective, *Paleoceanography*, *12*, 546–559, doi:10.1029/97PA01019.

Reid, J. L. (1997), On the total geostrophic circulation of the Pacific Ocean: Flow patterns, tracers, and transports, *Prog. Oceanogr.*, *39*, 263–352, doi:10.1016/S0079-6611(97)00012-8.

Ridgway, K. R., and J. R. Dunn (2003), Mesoscale structure of the mean East Australian Current System and its relationship with topography, *Prog. Oceanogr.*, *56*, 189–222, doi:10.1016/S0079-6611(03)00004-1.

Rintoul, S. R. (1998), On the origin and influence of Adelie Land bottom water, in *Ocean, Ice and Atmosphere: Interactions at the Antarctic Continental Margin*, edited by S. S. Jacobs and R. F. Weiss, pp. 151–171, AGU, Washington, D. C.

Schmieder, F., T. von Dobeneck, and U. Bleil (2000), The Mid-Pleistocene climate transition as documented in the deep South Atlantic Ocean: Initiation, interim state and terminal event, *Earth Planet. Sci. Lett.*, *179*(3–4), 539–549, doi:10.1016/S0012-821X(00)00143-6.

Shackleton, N. J. (1977), Carbon-13 in Uvigerina: Tropical rainforest history and the equatorial Pacific carbonate dissolution cycles, in *The Fate of Fossil Fuel CO_2 in the Oceans*, edited by N. R. Andersen and A. Malahoff, pp. 401–427, Plenum, New York.

Shackleton, N. J., and B. N. Opdyke (1973), Oxygen isotope and palaeomagnetic stratigraphy of equatorial Pacific core V28–238: Oxygen isotope temperatures and ice volumes on a 105 and 106 year scale, *Quat. Res.*, *3*, 39–55, doi:10.1016/0033-5894(73)90052-5.

Shackleton, N. J., A. Berger, and W. R. Peltier (1990), An alternative astronomical calibration of the lower Pleistocene timescale based on ODP Site 677, *Trans. R. Soc. Edinburgh Earth Sci.*, *81*, 251–261.

Sigman, D. M., and E. A. Boyle (2000), Glacial/interglacial variations in atmospheric carbon dioxide, *Nature*, *407*(6806), 859–869, doi:10.1038/35038000.

Sokolov, S., and S. Rintoul (2000), Circulation and water masses of the southwest Pacific: WOCE section P11, Papua New Guinea to Tasmania, *J. Mar. Res.*, *58*(2), 223–268, doi:10.1357/002224000321511151.

Talley, L. D. (2007), *Hydrographic Atlas of the World Ocean Circulation Experiment (WOCE)*, vol. 2, Pac. Ocean Int.World Ocean Circ. Exp. Proj. Off., Southampton, U. K.

Thompson, P. R., A. W. H. Bé, J. C. Duplessy, and N. J. Shackleton (1979), Disappearance of pink-pigmented Globigerinoides-Ruber at 120,000-Yr Bp in the Indian and Pacific oceans, *Nature*, *280*(5723), 554–558, doi:10.1038/280554a0.

Toggweiler, J. R. (1999), Variation of atmospheric CO_2 by ventilation of the ocean's deepest water, *Paleoceanography*, *14*, 571–588, doi:10.1029/1999PA900033.

Tsimplis, M. N., S. Bacon, and H. L. Bryden (1998), The circulation of the subtropical South Pacific derived from hydrographic data, *J. Geophys. Res.*, *103*(C10), 21,443–21,468, doi:10.1029/98JC01881.

Venuti, A., F. Florindo, E. Michel, and I. R. Hall (2007), Magnetic proxy for the deep (Pacific) western boundary current variability across the mid-Pleistocene climate transition, *Earth Planet. Sci. Lett.*, *259*(1–2), 107–118, doi:10.1016/j.epsl.2007.04.032.

Venz, K. A., and D. A. Hodell (2002), New evidence for changes in Plio-Pleistocene deep water circulation from Southern Ocean ODP Leg 177 Site 1090, *Palaeogeogr. Palaeoclimatol. Palaeoecol.*, *182*, 197–220, doi:10.1016/S0031-0182(01)00496-5.

Warren, B. A. (1973), Transpacific hydrographic sections at lats 43°S and 28°S: The SCORPIO Expedition–II. Deep water, *Deep Sea Res., Oceanogr. Abstr.*, *20*(1), 9–38.

Warren, B. A. (1981), Deep circulation of the world ocean, in *Evolution of Physical Oceanography*, edited by B. A. Warren and C. Wunsch, pp. 6–41, MIT Press, Cambridge, Mass.

Warren, B. A., T. Whitworth, M. I. Moore, and W. D. Nowlin (1994), Slight northwestward inflow to the deep south Fiji Basin, *Deep Sea Res., Part I*, *41*(5–6), 953–956, doi:10.1016/0967-0637(94)90086-8.

Whitworth, T., B. A. Warren, W. D. Nowlin, S. B. Rutz, R. D. Pillsbury, and M. I. Moore (1999), On the deep western-boundary current in the southwest Pacific Basin, *Prog. Oceanogr.*, *43*, 1–54, doi:10.1016/S0079-6611(99)00005-1.

Wijffels, S. E., J. M. Toole, and R. Davis (2001), Revisiting the South Pacific subtropical circulation: A synthesis of World Ocean Circulation Experiment observations along 32°S,

J. Geophys. Res., *106*(C9), 19,481–19,513, doi:10.1029/1999JC000118.

WOCE (2002), World Ocean Circulation Experiment: Global Data, Version 3.0, *Rep. 180/02*, Southampton, U. K.

Wyrtki, K. (1961), The flow of water into the deep sea basins of the western South Pacific Ocean, *Aust. J. Mar. Freshwater Res.*, *12*, 1–16, doi:10.1071/MF9610001.

Zahn, R., K. Winn, and M. Sarnthein (1986), Benthic foraminiferal $\delta^{13}C$ and accumulation rates of organic carbon: *Uvigerina peregina* group and *Cibicidoides wuellerstorfi*, *Paleoceanography*, *1*, 27–42, doi:10.1029/PA001i001p00027.

G. Cabioch, LOCEAN, UMR 7159, IRD, UPMC, MNHN, CNRS, 32 Avenue Henri Varagnat, F-93143 Bondy CEDEX, France.

T. Corrège, Environnements et Paléoenvironnements Océaniques, Université de Bordeaux, UMR 5805, Avenue des Facultés, Bordeaux, F-33000, France.

P. De Deckker, Research School of Earth Sciences, Australian National University, Canberra, ACT 0200, Australia.

M. Elliot and T. Russon, School of Geosciences, University of Edinburgh, UK. (t.f.russon@sms.ed.ac.uk)

C. Kissel, Laboratoire des Sciences du Climat et de l'Environnement, IPSL, Laboratoire Mixte CEA-CNRS-UVSQ, Parc du CNRS, Avenue de la Terrasse, F-91198 Gif-sur-Yvette CEDEX, France.